Innate immune signaling in trophoblast and decidua organoids defines differential antiviral defenses at the maternal-fetal interface

Liheng Yang[1], Eleanor C. Semmes[1,2], Cristian Ovies[1], Christina Megli[3,4], Sallie Permar[5], Jennifer B. Gilner[6], Carolyn B. Coyne[1,2*]

[1]Department of Molecular Genetics and Microbiology, Duke University School of Medicine, Durham, NC USA, [2]Duke Human Vaccine Institute, Duke University, Durham, NC, USA, [3]Division of Maternal-Fetal Medicine, Division of Reproductive Infectious Disease, Department of Obstetrics, Gynecology and Reproductive Sciences, University of Pittsburgh Medical Center (UPMC), [4]Magee Womens Research Institute, Pittsburgh, PA USA, [5]Department of Pediatrics, Weill Cornell Medical Center, and [6]Division of Maternal-Fetal Medicine, Department of Obstetrics and Gynecology, Duke University Medical Center, Durham, NC.

*Address correspondence
Carolyn Coyne, PhD
3130 Medical Sciences Research Building III
3 Genome Court
Durham, NC 27710
USA
carolyn.coyne@duke.edu

Abstract

Infections at the maternal-fetal interface can directly harm the fetus and induce complications that adversely impact pregnancy outcomes. Innate immune signaling by both fetal-derived placental trophoblasts and the maternal decidua must provide antimicrobial defenses at this critical interface without compromising its integrity. Here, we developed matched trophoblast and decidua organoids from human placentas to define the relative contributions of these cells to antiviral defenses at the maternal-fetal interface. We demonstrate that trophoblast and decidua organoids basally secrete distinct immunomodulatory factors, including the constitutive release of the antiviral type III interferon IFN- λ2 from trophoblast organoids, and differentially respond to viral infections through the induction of organoid-specific factors. Lastly, we define the differential susceptibility of trophoblast and decidua organoids to human cytomegalovirus (HCMV) and the transcriptional and immunological responses of these organoids to HCMV infection. Our findings establish matched trophoblast and decidua organoids as *ex vivo* models to study vertically transmitted infections and highlight differences in innate immune signaling by fetal-derived trophoblasts and the maternal decidua.

Introduction

The maternal-fetal interface is comprised of both the maternal-derived decidua and the fetal-derived placenta, which together support fetal growth, maintain maternal-fetal immunotolerance, and provide immunologic defenses to protect the fetus from infections. The relative contributions of maternal- and fetal-derived cells to these critical functions remain largely undefined given the limitations of models that recapitulate the complex nature of the human maternal-fetal interface.

The fetal-derived placenta contains distinct trophoblast subsets throughout gestation. Trophoblast stem cells located in chorionic villi, the branch like projections that directly contact maternal blood, give rise to cytotrophoblasts (CTBs), the proliferative mononuclear cells of the placenta, the syncytiotrophoblast (STB), a multinucleated contiguous cell layer that covers the villous surfaces, and extravillous trophoblasts (EVTs). EVTs remodel the maternal microvasculature to form spiral arteries, which ultimately deliver maternal blood to the surface of chorionic villi. On the maternal side, decidualization of the endometrium is required for implantation and appropriate placentation. Together, the decidua and placenta maintain immunotolerance throughout gestation and provide the fetus with essential hormones and nutrients to support its growth.

While the placenta and decidua play complementary roles in fetal development, their contributions to antimicrobial defenses are less defined [1, 2]. The placenta forms a formidable barrier to infections, yet certain congenital pathogens (e.g., *Toxoplasma gondii*, Zika virus (ZIKV), HIV, Rubella, and Human Cytomegalovirus (HCMV)) can be vertically transmitted to infect the fetus and in some cases, cause disease and/or pregnancy loss. Studies of tissue explants and histopathologic analysis of the placenta suggest that the decidua and chorionic villi have differing roles in the pathogenesis of infections. The decidua may be a primary site of replication for several microorganisms associated with congenital disease, including HCMV [3-5], ZIKV [6-8], and *Listeria monocytogenes* [9], suggesting it may serve as a reservoir for these infections. By contrast, the placenta is largely resistant to infections and possesses intrinsic mechanisms of innate immune defense. For example, human trophoblasts constitutively release antiviral interferons (IFNs) that

53 restrict infection in both autocrine and paracrine manners [10, 11]. These IFNs are of the type III
54 class, which include IFNs-λ1-3 in humans [12, 13]. Constitutive release of IFNs is a unique feature
55 of trophoblasts as IFNs are tightly regulated in most cell types and induced only after detection of
56 the products of viral replication. Together, these findings suggest that maternal- and fetal-derived
57 tissue differentially respond to and control viral infections; however, the lack of available models to
58 fully interrogate the differences between maternal- and fetal-derived cells has limited a complete
59 understanding of their respective roles in antiviral defense.

60 The paucity of tractable models to study the human maternal-fetal interface and the limitation
61 of accessing this interface *in vivo* without disrupting pregnancy has limited our understanding of the
62 pathogenesis of and immune responses against many congenital pathogens, including HCMV.
63 HCMV is a species-specific and host-restricted β-herpesvirus that can only infect humans, and
64 animal models using guinea pig (GPCMV) or rhesus macaque (RhCMV) cytomegaloviruses rely on
65 viruses that are genetically disparate from HCMV and do not fully recapitulate the human decidua-
66 placenta interface [14]. Prior studies on placental HCMV infection have used trophoblast progenitor
67 cells, EVT cell lines, and primary trophoblasts; however, these cell lines and isolated primary cells
68 do not model the cellular complexity of the human placenta [15]. Placental and decidual explants
69 have also been employed to model HCMV infection, yet these human explants have high inter-
70 individual variability, which hinders reproducibility, and a limited window of viability in cultured *ex vivo*
71 tissue [4, 6, 16]. Therefore, novel models of the human maternal-fetal interface are needed to
72 understand the contributions of maternal decidual cells and fetal-derived placental cells to immune
73 defense and pathogenesis of placental HCMV infection.

74 The recent development of trophoblast and decidua organoids from first trimester placental
75 tissue has greatly expanded the models available to study the human maternal-fetal interface [17,
76 18]. Previous work has shown that isolation and propagation of trophoblast stem cells from first
77 trimester placental chorionic villi leads to the development of three-dimensional organoids that
78 differentiate to contain all lineages of trophoblast cells present in the human placenta and release

well-known pregnancy hormones such as human chorionic gonadotropin (hCG) [17]. Similarly, decidua organoids isolated from uterine glands recapitulate the transcriptional profile of their tissue of origin and respond to hormonal cues [18]. These organoid models are ideal to interrogate differences between maternal- and fetal-derived cells; however, decidua and trophoblast organoids have not yet been used to model congenital infections.

To directly compare antiviral signaling pathways between the human placenta and decidua, we generated trophoblast and decidua organoids from matched mid-to-late gestation (26-41 weeks of gestation) human placentas and profiled their release of cytokines, chemokines, and other factors at baseline and under virally infected conditions. These studies revealed that trophoblast organoids basally secrete the IFN-λ2, which does not occur in matched decidua organoids. To determine whether maternal- and fetal-derived cells respond differently to viral infections, we compared the transcriptional profiles and immunological secretomes from organoids treated with a ligand to stimulate toll-like receptor 3 (TLR3) signaling. Trophoblast and decidua organoids differentially responded to TLR3 activation through the secretion of organoid-specific cytokines and chemokines. Lastly, we defined the differential susceptibility of trophoblast and decidua organoids to HCMV infection and identified key differences in the innate immune responses of these organoids to HCMV infection. Together, these studies highlight the differential responses of decidual and placental cells at the maternal-fetal interface to viral infections and provide new models to understand innate immune responses against placental infections.

Results

Establishment and characterization of human trophoblast and decidual organoids from mid-to-late gestation tissue

To generate matched human trophoblast organoids (TOs) and decidual organoids (DOs), we used human placental tissue isolated from the second and third trimesters of human pregnancy (26-41 weeks gestation) and cultured progenitor cells isolated from chorionic villi or decidua (**Figure 1A**).

105 Given that previous work developed TOs utilizing tissue isolated from the first trimester [17-22], we
106 optimized the isolation and propagation procedures for isolation of cells from mid-to-late gestation
107 chorionic villi. This optimization included extended mechanical disruption of tissue and the addition
108 of supplements including nicotinamide to promote progenitor cell differentiation. Although the
109 abundance of trophoblast stem/progenitor cells decreases after the first trimester [17], we
110 successfully isolated progenitor cells and generated organoids from all placental tissue harvested
111 (eleven unique placentas). Consistent with the presence of progenitor cells in full-term chorionic villi,
112 we identified cells positive for the proliferation marker Ki67 in villi isolated from two late gestation
113 placental villi used to generate TOs (**Supplemental Figure 1A**). Isolated progenitor cells were
114 embedded in Matrigel to allow for self-organization and propagated for ~2-3 weeks to generate
115 organoid structures that were morphologically like those previously isolated from first trimester
116 placentas [17, 18] (**Figure 1B, Supplemental Figure 1B**). Once established, organoids could be
117 continuously expanded and passaged every 3-5 days for DOs and 5-7 days for TOs and were highly
118 proliferative based on Ki67 immunostaining (**Supplemental Figure 1C)**. Confocal microscopy for
119 cytoskeletal and adhesion markers including cytokeratin-19, actin, E-cadherin, and the Epithelial Cell
120 Adhesion Molecule (EpCAM) confirmed the three-dimensional architecture of established organoids
121 and verified that TOs and DOs expressed markers consistent with their tissues of origin (**Figure 1C,**
122 **1D** and **Supplemental Figure 1D**). This also included the expression of the trophoblast-specific
123 marker Sialic Acid Binding Ig Like Lectin 6 (SIGLEC6) in TOs but not DOs and the expression of the
124 mucin MUC5AC in DOs but not TOs (**Figure 1C, 1D** and **Supplemental Figure 1D)**. In addition, we
125 confirmed that TOs differentiated to multiple lineages of trophoblast cells and a subset of cells were
126 positive for the EVT specific marker HLA-G (**Figure 1C, Supplemental Figure 1D**). We also found
127 that TOs, but not DOs, secreted the trophoblast-specific hormone hCG as assessed by Luminex
128 assays and OTC test strips (**Figure 1E**). The levels of hCG were stable in TOs propagated for
129 extended periods of time (**Figure 1F**). In addition, we confirmed that DOs released high levels of the
130 secreted mucin MUC16 as determined by Luminex assays, which was not present in TOs (**Figure**

131 **1G**). Collectively, these data show that TOs and DOs are morphologically and functionally distinct
132 and that they recapitulate human placental trophoblasts and decidua glandular epithelial cells.
133
134 **Distinct transcriptional profiles in TOs and DOs as assessed by RNASeq**
135 Next, we performed transcriptional profiling of established TO and DO lines using bulk RNASeq. We
136 found that TOs and DOs were transcriptionally distinct based on differential expression analysis
137 using DESeq2 followed by principal component analysis (PCA) (**Figure 2A**, **Supplemental Figure**
138 **2A, 2B, 2C**). TOs highly expressed transcripts specifically enriched in the placenta, including
139 HSD3B1, XAGE2 and 3, GATA3, and ERVW-1, which were absent or expressed at very low levels
140 in DOs (**Figure 2B, Supplemental Figure 2C, 2D, 2E**). In addition, TOs highly expressed transcripts
141 for PSGs, ERVW-1, and CGA, which were not expressed in DOs (**Figure 2B**). The levels of
142 expression of these transcripts were similar to those in primary human trophoblasts (PHTs),
143 confirming that TOs recapitulate the transcriptional signature of primary trophoblasts (**Figure 2B**).
144 These markers were consistent with the presence of the STB (e.g., CGA, PSGs, HSD3B1), CTBs
145 (e.g., TP63), and EVTs (e.g., ITGA5) (**Figure 2B**). In contrast, DOs expressed markers associated
146 with the decidua and decidual stromal cells, including MUC1, MUC5A, MUC5B, SOX17, and HOXB8
147 which were absent or expressed at low levels in TOs and PHT cells (**Figure 2B, Supplemental**
148 **Figure 2F, 2G**). To further confirm that TOs and DOs recapitulated their tissues of origin, we profiled
149 the expression of three members of the chromosome 19 microRNA family (C19MC), which are
150 specifically expressed in the human placenta [23]. We found that miR-516B-5p, miR-517A-3p, and
151 miR-525-5p were expressed at high levels in TOs, comparable to levels observed in freshly isolated
152 chorionic villi, but were not expressed in DOs (**Figure 2C**). Lastly, we found that TOs isolated from
153 placentas obtained from male fetuses expressed Y-linked genes, which were absent in female-only
154 derived DOs (**Supplemental Figure 2H**). Collectively, these data establish matched TOs and DOs
155 as model systems of the maternal-fetal interface and demonstrate that they can be isolated from
156 tissue after the first trimester, including from mid-to-late gestation.

157

158 **Comparative immune secretome profiling of TOs and DOs**

159 We have shown previously that human chorionic villous explants release numerous cytokines,
160 chemokines, and growth factors that impact both maternal and fetal antimicrobial defenses [11, 24].
161 Similarly, we have shown that PHTs isolated from mid-gestation and full-term placentas secrete
162 some of these same immunomodulatory factors [11, 24]. We therefore profiled the immunological
163 secretome of matched TOs and DOs isolated from independent placentas to define basal differences
164 in the secretome of cells that comprise the maternal-fetal interface. To do this, we used multianalyte
165 Luminex-based profiling of 105 cytokines, chemokines, growth and other factors from conditioned
166 media (CM) isolated under basal unstimulated conditions. Factors whose secretion was reliably
167 measured over 50pg/mL were defined as present in CM. We found that TOs secreted only two
168 cytokines (IL-6 and IL-28A/IFN-λ2) and three immune-regulated secreted soluble receptors (sTNF-
169 R1, gp130/sIL-6Rβ, sTNF-R2) at baseline (**Figure 3A**). By contrast, DOs released a larger number
170 of immune factors overall, with 21 detected in DO-derived CM at baseline (**Figure 3B**). PCA of these
171 Luminex profiles identified factors contributing to the differential nature of the secretome between
172 TOs and DOs, which included the enrichment of factors including CXCL1, CXCL5, and IL-8 in DOs
173 versus IL-6 and IL28A/IFN-λ2 in TOs (**Figure 3C-F**). Together, these data define the unique
174 immunologic secretome of key cells that comprise the maternal-fetal interface.

175

176 **Trophoblast organoids constitutively secrete antiviral IFN-λ2**

177 We showed previously that PHT cells isolated from full-term placentas and mid-gestation chorionic
178 villi constitutively release type III IFNs, which protect trophoblasts from viral infections [10, 11]. We
179 found that TOs recapitulated this phenotype and released high levels of IFN-λ2, but not type I IFNs
180 or IFN-λ1 (**Figure 4A**). In contrast, DOs did not basally secrete any detectable IFNs (**Figure 4B**).
181 The levels of released IFN-λ2 were comparable to those from PHT cells and from matched cultured
182 villous explants (**Figure 4C**). Consistent with the specific constitutive release of IFN-λ2 from TOs,

183 the expression of transcripts associated with type III IFNs was high in TOs compared to DOs (**Figure**
184 **4D**). We monitored the release of IFN-λ2 over the growth period of TOs and found that it's release
185 was detectable by ~10-days post-plating and reached high levels by >14-days in culture, which
186 correlated with similar trends for IL-6 (**Supplemental Figure 3**). We confirmed that CM isolated from
187 TOs, but not DOs, induced interferon stimulated genes (ISGs) in cells treated with this CM using a
188 HEK293 based reporter assay (**Figure 4E**). Consistent with this, we found that CM isolated from
189 TOs was antiviral and reduced ZIKV infection in CM-treated non-placental cells (**Figure 4F**),
190 confirming that TO-derived CM exerts potent antiviral effects on non-placental cells.
191

192 **Differential induction of cytokine and chemokine networks in TOs and DOs in response to**
193 **poly I:C treatment**

194 Because we observed differences in the basal secretomes of TOs and DOs, we next determined
195 whether TOs and DOs differentially respond to viral infections. To do this, we used poly (I:C), a
196 synthetic ligand of TLR3, and profiled the transcriptional and secretory changes induced by poly I:C
197 treatment of TOs and DOs. We found that both TOs and DOs robustly responded to poly I:C
198 treatment, which corresponded with significant transcriptional changes as assessed by RNASeq
199 (**Figure 5A**, **5B**). Comparison of the transcripts induced by poly I:C treatment (as defined by
200 significance of $p<0.01$ and $\log_2$ fold-change of +/- 2) of TOs and DOs revealed that TOs upregulated
201 448 transcripts whereas DOs upregulated 121 (**Supplemental Figure 4A**). Of these, only 69 were
202 shared between TOs and DOs, the majority of which (64 of 69) were ISGs (**Supplemental Figure**
203 **4A, 4B)**. Of the differentially induced transcripts, TOs induced the expression of chemokines
204 including CXCL5 ($\log_2$ fold change 5.9), CX3CL1 ($\log_2$ fold change 7.1), and CCL22 ($\log_2$ fold change
205 7.6), which were the most induced cytokine or chemokine transcripts in poly I:C-treated TOs (**Figure**
206 **5C**). In contrast, DOs expressed chemokines at high basal levels, which were not further induced by
207 poly I:C treatment and did not induce any CCL22 (**Figure 5C**). Transcripts most selectively induced
208 in DOs included CD38 and the phospholipase PLA1A (**Figure 5C**).

209 To confirm the transcriptional changes described above, we performed parallel multianalyte
210 Luminex profiling of 105 cytokines and chemokines in TOs and DOs treated with poly I:C. Both TOs
211 and DOs mounted robust responses to poly I:C treatment that correlated with the release of high
212 levels of select cytokines and chemokines (**Figure 5D**). Cytokines and chemokines with levels >5-
213 fold above baseline were defined as induced by poly I:C treatment. The topmost induced factors in
214 poly I:C-treated TOs were the chemokines CCL22, CXCL5, CXCL2, and CX3CL1 (**Figure 5D, left**),
215 which was consistent with their transcriptional upregulation by RNASeq (**Figure 5C**). PCA of
216 Luminex-based profiling of poly I:C treated TOs and DOs revealed organoid-specific responses to
217 this treatment, which included the specific induction of CCL22 in poly I:C treated TOs (**Supplemental**
218 **Figure 4C**, **Figure 5E, 5F**). Factors induced by both TOs and DOs included the type III IFNs IFN-λ1
219 and IFN-λ2 (**Figure 5G, 5H**), which were the top-most induced factors in DOs. In contrast, the type
220 I IFNs IFN-α2 and IFNβ were induced to significantly greater levels in TOs than DOs (**Supplemental**
221 **Figure 4D, 4E**). Other chemokines induced in TOs were basally expressed at high levels in DOs and
222 were not further induced by poly I:C (**Supplemental Figure 4F-J**).
223

224 **Differential susceptibility of TOs and DOs to HCMV infection**

225 HCMV is the most common vertically transmitted pathogen and is associated with high rates of
226 congenital disease, yet how HCMV transmits across the placenta and how the maternal decidua and
227 fetal-derived placenta respond to HCMV infection remains poorly defined. To address these
228 questions, we infected TOs and DOs with HCMV strains AD169r (BADrUL131-Y4, tagged with GFP
229 [25]) and TB40E (tagged with mCherry [26]). We found that DOs were highly permissive to HCMV
230 infection as quantified by detectable GFP or mCherry expression of viral gene expression in the
231 majority of organoids (**Figure 6A, 6C, 6D**). In contrast, TOs were largely resistant to HCMV infection,
232 with low levels of infection by AD169r and almost undetectable levels by TB40E, as assessed by
233 fluorescence of tagged viral gene expression (**Figure 6B, 6C, 6D).** Because we observed minimal
234 HCMV infection in TOs, we next sought to determine whether the low levels of HCMV infection we

235 observed occurred in EVTs, which have been proposed as possible targets of many teratogenic
236 viruses including HCMV [1]. To do this, we quantified the extent of overlap between AD169r infection
237 as assessed by GFP expression and HLA-G, an EVT specific marker. We found that there was
238 almost no overlap between GFP and HLA-G, suggesting that EVTs may not be the primary targets
239 of HCMV infection in TOs (**Figure 6E, 6F**).
240

241 **Differential transcriptional responses of TOs and DOs to HCMV infection**

242 Because we observed significant differences between the susceptibility of TOs and DOs to HCMV
243 infection, we next profiled the transcriptional changes induced by HCMV infection in these organoids.
244 Matched TOs and DOs were infected with AD169r or TB40E strains of HCMV and the effects of this
245 infection was assessed by bulk RNASeq transcriptional profiling. TOs responded to HCMV infection
246 through the differential expression of 282 transcripts (AD169r strain) or 173 transcripts (TB40E
247 strain), of which ~38% were shared between both strains of HCMV (**Figure 7A, 7C**). By contrast,
248 DOs responded to HCMV infection less robustly, with 95 (AD169r strain) or 117 (TB40E strain)
249 transcripts differentially expressed by this infection (**Figure 7B, 7D**). Of these differentially expressed
250 transcripts, only 3-4% were shared between TOs and DOs infected with AD169r (**Figure 7E**) or
251 TB40E (**Figure 7F**). Of these shared transcripts, only three were induced by both strains of HCMV
252 in both TOs and DOs and included CCNA1 (Cyclin A1), the ISG OAS2, and EPSTI1 (Epithelial
253 Stromal Interaction 1) (**Figure 7G**). Transcripts specifically induced by HCMV infection of TOs
254 included H3Y1 (H3.Y Histone 1), KHDC1L (KH Domain Containing 1 Like), several members of the
255 PRAME Family (PRAMEF2, 8, 12, 14, and 20), and TRIM49A and B (Tripartite Motif Containing 43)
256 (**Figure 7H**). In contrast, DO-specific transcripts included several components of the nitric oxide
257 signaling pathway including NOS2 (Nitric Oxide Synthase 2), DUOX2 (Dual Oxidase 2), and
258 DUOXA2 (Dual Oxidase Maturation Factor 2) as well as CXCL10 and CSF3/G-CSF (**Figure 7I**).
259

260 **Differential immune secretome of TOs and DOs infected with HCMV**

261

262 To define the innate immune responses to HCMV infections in TOs and DOs, we used Luminex
263 multianalyte assays of >100 cytokines and chemokines in TOs and DOs infected with HCMV strains
264 AD169r or TB40E. We found that TOs responded to HCMV infection by the secretion of relatively
265 few cytokines, which included pentraxin-3 (PTX3), first described as an endothelial factor induced
266 by IL-1β treatment [27], IL-8, and IL-11 (**Figure 8A, 8C, 8D, Supplemental Figure 5A**). In contrast,
267 DOs responded to HCMV infection through the secretion of both proinflammatory cytokines and
268 chemokines (e.g., CXCL10, MIP-1α, MIP-1β, IL-6) and through the release of the type III IFN IFN-
269 λ2 (**Figure 8B, 8C, 8E-F**, **Supplemental Figure 5B**). In contrast to IFN-λ2, DOs did not induce any
270 other detectable IFNs such as IFN-α2 or IFN-β or IFN- λ1 (**Figure 8B**, **8G-I**). Together, these findings
271 highlight the distinct immunoregulatory and transcriptional cascades induced by HCMV infection of
272 decidual versus placental cells that comprise the human maternal-fetal interface.

273

274 **Discussion**

275 Our work establishes fetal- and maternal-derived organoids as models for defining innate
276 immune signaling at the maternal-fetal interface. Similar to PHTs [10] and mid-gestation chorionic
277 villi [11], we show that TOs constitutively secrete type III antiviral IFN-λ, that act in paracrine to restrict
278 viral infections. In contrast, although DOs did not basally secrete IFNs, they are immunologically
279 more active under resting conditions and basally secrete cytokines and chemokines not detectable
280 in TOs. In addition, we show that TOs and DOs respond to TLR3 activation via the induction of
281 distinct immune regulatory networks, which includes the specific release of select chemokines such
282 as CCL22 in TOs. Lastly, we used matched TOs and DOs to explore differences in susceptibility to
283 HCMV and to define the differential responses of the maternal decidua and fetal-derived organoids
284 to HCMV infection. Taken together, our work suggests that cells that comprise the maternal-fetal

285 interface defend from viral infections in a cell-type specific manner and further highlight the unique
286 contributions of fetal-derived trophoblasts in antiviral immunity.

287 The previous establishment of trophoblast and decidua-derived organoids has significantly
288 expanded the *in vitro* systems that can model the complexity of the maternal-fetal interface [17, 18].
289 These previous studies utilized tissue isolated from the first trimester of pregnancy (6-9 weeks
290 gestation for TOs and 8-12 weeks gestation for DOs) [17, 18], although another study successfully
291 established DOs from full-term tissue [22]. Two-dimensional cultures of stem cell-derived primary
292 trophoblasts were also obtained from the first trimester [20]. The placenta is a dynamic organ that
293 changes throughout gestation. Here, we show that TOs can also be generated from later stages of
294 gestation, including from progenitor cells isolated in the second and third trimesters of pregnancy
295 and full-term placental tissue, which required optimization from conditions required for first trimester
296 tissue. Although the abundance of progenitor cells, as defined by the presence of Ki67 positive
297 nuclei, declines throughout gestation, we show that full-term chorionic villi contain Ki67 positive cells
298 at low levels and that these cells can be isolated to generate organoids. Given that obtaining first
299 trimester tissue can be complicated by access and/or regulatory restrictions, our study provides an
300 additional source for the development of placental organoids from tissue obtained later in gestation.
301 In addition, given that many congenital infections occur in the second and third trimesters of
302 pregnancy, organoids isolated from later stages of pregnancy may better reflect clinically relevant
303 models of congenital infections. For instance, the risk of transplacental transmission of HCMV
304 infection from mother-to-fetus is only 20% in the first trimester but can reach up to 75% in the third
305 trimester, highlighting the relevance of our organoid model for studying placental HCMV infection
306 across gestation [28].

307 Unlike many other barrier cell types such as the epithelium, human trophoblasts have the
308 unique capacity to robustly secrete cytokines and other immunological factors without stimulation.
309 PHTs from full-term placentas and mid-gestation chorionic villi secrete cytokines that mediate innate
310 immune defenses against bacteria, parasites, and viruses [10, 24, 29]. Consistent with this concept,

311 serum isolated from pregnant women often contains elevated levels of these cytokines, indicating
312 that at least some have reached the systemic circulation [24, 30-32]. Similarly, the decidua releases
313 specific cytokines and alterations in these profiles may be associated with pregnancy complications
314 including miscarriage [33-38]. The decidua also responds to microbial infections via the release of
315 additional cytokines that function in innate defense [7, 39, 40]. However, in many cases, these
316 studies were performed on tissue explants that were multicellular in nature, thus preventing an
317 assessment of the contributions of cytokine release from distinct cell types. Similarly, previous work
318 utilizing tissue explants that were treated with recombinant cytokines, synthetic ligands of various
319 innate immune pathways, or infected with pathogens are also unable to define the contributions of
320 distinct cell types in these responses. The use of organoids allows for analyses of cellular responses
321 to infection or innate immune activation from trophoblasts and decidual glands in primary cell models
322 that contain isolated cell types enriched at the maternal-fetal interface. An additional strength of the
323 TO model is that trophoblast stem cells can differentiate into all three distinct trophoblast cell types
324 comprising the human placenta, which is not possible in many other existing models including
325 isolation of CTBs from full-term placentas, which do not differentiate to contain EVTs.

326 The constitutive release of IFN-λs from human trophoblasts is a unique phenomenon that
327 runs counter to much of what is known about antiviral IFN signaling, which is centered on a
328 requirement for viral sensing as a prerequisite to induce this pathway. Similar to our previous studies
329 in PHT cells and mid-gestation chorionic villous explants [10, 11], our data show that progenitor cell-
330 derived TOs also constitutively release IFN-λs. Our studies also show that type III IFNs are further
331 induced by activation of antiviral innate immune signaling in both TOs and DOs, with IFN-λs being
332 amongst the most induced cytokines detected in both organoid types. Although IFNs are released
333 from TOs constitutively and upon induction of antiviral signaling, our studies also point to select
334 chemokines as key components in the responses of the human placenta to viral infections. We show
335 that the regulatory T cell (Treg) chemoattractant CCL22 is selectively released from TOs in response
336 to TLR3 activation. We have shown previously that human PHTs and mid-gestation chorionic villi

337 also respond to *T. gondii* infection through the selective release of CCL22 [29, 41], suggesting that
338 this chemokine may be key mediator of the response of the human placenta to microbial infections.
339 Given that Treg infiltration into the decidua has been associated with adverse pregnancy outcomes
340 including miscarriage [42], CCL22 induction may directly impact maternal-fetal tolerance and
341 adversely impact fetal health.

342 Understanding congenital HCMV transmission and innate immune defenses against HCMV
343 infection at the maternal-fetal interface has been greatly hindered by a lack of model systems and
344 has relied heavily on first trimester explant tissues to-date. Our work highlights that trophoblast and
345 decidua organoids derived from mid-to-late gestation tissue can be leveraged as an accessible
346 model system for studying HCMV infection at the maternal-fetal interface. Our finding that DOs were
347 highly susceptible to HCMV infection is consistent with prior work in first trimester decidua explants
348 demonstrating that HCMV productively infects the maternal decidua, which may function as a viral
349 reservoir for HCMV [4, 43]. Using trophoblast and decidua organoids, we found that DOs had
350 heightened susceptibility to HCMV infection compared to matched TOs. This finding of elevated
351 decidual susceptibility to HCMV has important implications, as an improved understanding of the
352 pathogenesis of viral transmission *in utero* will be key to developing effective interventions to prevent
353 congenital infection. Our transcriptional and Luminex-based profiling also revealed that HCMV-
354 infected TOs and DOs differentially respond to this infection through organoid-specific transcriptional
355 signatures and cytokine and chemokine signaling networks. For example, CXCL10 was highly
356 upregulated in HCMV-infected DOs by both RNASeq and Luminex-based profiling, which is
357 consistent with prior findings of elevated CXCL10 in the amniotic fluid of HCMV-transmitting women
358 [44] and in *ex vivo* infections of decidua explants [6, 43]. Moreover, the induction of IL-8 in HCMV-
359 infected TOs mirrors the IL-8 secretion observed previously in response to HCMV infection of
360 isolated first trimester trophoblasts [45] and placental explants [6]. That our *in vitro* organoid
361 infections recapitulated innate immune responses previously observed *in vivo* and *ex vivo* further

validates our model of matched decidua and trophoblast organoids for studying HCMV and other vertically transmitted pathogens.

Our work presented here develops TOs and DOs from mid-to-late gestation placental tissue and demonstrates that these organoids can be used to study mechanisms of microbial vertical transmission and antiviral innate immune signaling. We show that TOs and DOs constitutively secrete unique cytokines and chemokines and respond to viral infections through the release of organoid-specific immunomodulatory factors. Our work also highlights the prominent role of type III IFNs in antiviral immunity at the maternal-fetal interface and demonstrates that TOs constitutively release IFN-λs and that DOs can be induced to release IFN-λs following viral infection. Collectively, these studies define the differential responses of decidual and placental cells comprising the maternal-fetal interface to viral infections and suggest that organoid-based models can be used to define innate immune signaling at this interface.

Materials and Methods

Human samples. Human tissue used in this study was obtained through the UPMC Magee-Womens Hospital Obstetric Maternal & Infant Database and Biobank or from Duke University after approval was received from the University of Pittsburgh or Duke University Institutional Review Board (IRB) and in accordance with the guidelines of the University of Pittsburgh and Duke University human tissue procurement. Placental tissue used in this study was collected from the second (23rd-27th weeks) and third (35th- 41st weeks) trimesters. Placental tissue was excluded for diagnosis of PPROM or maternal infection.

Derivation and culture of trophoblast organoids (TO) from human placental samples. Villous trophoblast stem/progenitor cells were isolated from fresh placental tissues as described previously with further optimization based on the characteristics of late gestation placenta villi [17]. Briefly, villi collected from fresh placental tissue were intensively washed, then were sequentially digested with

388 0.2% trypsin-250 (Alfa Aesar, J63993-09)/0.02% EDTA (Sigma-Aldrich, E9884-100G) and 1.0
389 mg/mL collagenase V (Sigma-Aldrich, C9263-100MG) and further mechanically disrupted by
390 pipetting up and down vigorously ~10 times with 10 ml serological pipette. Pooled digests were
391 washed with Advanced DMEM/F12 medium (Gibco 12634-010) and pelleted by centrifugation, then
392 resuspended in approximate 10 times volume of ice-cold growth-factor-reduced Matrigel (Corning
393 356231). Matrigel "domes" (40 µl/well) were plated into 24-well tissue culture plates (Corning 3526),
394 placed in a 37°C incubator to pre-polymerize for ~3 min, turned upside down to ensure equal
395 distribution of the isolated cells in domes for another 10 min, then carefully overlaid with 500 µL
396 prewarmed trophoblast organoid medium (TOM) consisting of Advanced DMEM/F12 (Life
397 Technologies, 12634-010) supplemented with 1× B27 (Life Technologies, 17504-044), 1× N2 (Life
398 Technologies, 17502-048), 10% FBS (vol/vol, Cytiva HyClone, SH30070.03), 2 mM GlutaMAX™
399 supplement (Life Technologies, 35050-061), 100 µg/mL Primocin (InvivoGen, ant-pm-1), 1.25 mM
400 N-Acetyl-L-cysteine (Sigma, A9165), 500 nM A83-01 (Tocris, 2939), 1.5 µM CHIR99021 (Tocris,
401 4423), 50 ng/mL recombinant human EGF (Gibco, PHG0314), 80 ng/mL recombinant human R-
402 spondin 1 (R & D systems, 4645-RS-100), 100 ng/mL recombinant human FGF2 (Peprotech, 100-
403 18C), 50 ng/mL recombinant human HGF (Peprotech, 100-39), 10mM nicotinamide (Sigma, N0636-
404 100G), 5 µM Y-27632 (Sigma, Y0503-1MG), and 2.5 µM prostaglandin E2 (PGE2, R & D systems,
405 22-961-0). Cultures were maintained in a 37°C humidified incubator with 5% CO_2. Medium was
406 renewed every 2-3 days. Small trophoblast organoid spheroids became visible by approximately day
407 12 post-isolation. Derived TOs were passaged every 5 to 7 days depending on their size and density.
408 To passage, TOs were released from domes with ice-cold cell recovery solution (Corning, 354253)
409 and then were digested in prewarmed TrypLE Express (Gibco, 12605-028) or Stem Pro Accutase
410 (Gibco, A11105-01) at 37°C for 5-7 min. Further mechanical dissociation was achieved with an
411 Eppendorf Explorer Plus electronic pipettes at its "mix" function setting by pipetting up and down
412 around 400 times through small-bore pipette tips. Dissociated TOs fragment were collected and
413 washed by centrifuge, then resuspended in fresh ice-cold Matrigel and replated as domes at the

414 desired density for continuous culture. For freezing TOs, overlaid TOM was aspirated, TOs with
415 Matrigel were resuspended in CryoStor CS10 stem cell freezing medium (STEMCell Technologies,
416 07930) frozen at -80 ℃ and then transferred to liquid nitrogen for long-term storage. For thawing
417 cryopreserved TOs, organoids were thawed as quickly as possible, diluted with 5 times volume of
418 basic TOM containing Advanced DMEM/F12, 2 mM GlutaMAX supplement, 10 mM HEPES (Gibco,
419 15630-106), 1 × Penicillin/Streptomycin (Lonza, 17-602E) and centrifuged to pellet. Afterwards, TOs
420 were resuspended in new ice-cold Matrigel and replated for recovery culture and passaged as
421 described below.
422
423 **Derivation and culture of decidual organoids (DOs) cultures from human decidua samples**.
424 Decidual gland-enriched cell suspension were acquired from fresh decidual tissue as described
425 previously [18, 46]. Briefly, isolated decidual tissues were cut into small pieces then digested in 1.25
426 U/mL Dispase II (Sigma, D4693)/0.4 mg/mL collagenase V (Sigma, C-9263) solution. Glandular cells
427 were filtered out from the digestion solution supernatant and resuspended in ice-cold Matrigel
428 (Corning, 356231), plated as domes in 24-well plates (Corning 3526), and finally overlaid with 500
429 μL prewarmed organoid Expansion Medium (ExM) with the same composition as previously
430 described[18]. The growth medium was renewed every 2-3 days. Mature organoids were passaged
431 by mechanically disruption following TrypLE Express (Gibco, 12605) digestion every 3-5 days. Other
432 maintenance were similar to those as previously described [46].
433
434 **Generation of TO and DO conditioned media (CM).** Overlaid TOM and ExM were collected every
435 2-4 days based on the growth status of TOs and DOs. Media from at least ten timepoints for each
436 established organoid lines were collected as TO-CM or DO-CM. Non-conditioned medium (NCM)
437 was TOM or ExM (described above) that had not been exposed to TOs or DOs, respectively.
438

439 **Cells and Viral Infections.** Human osteosarcoma U2OS (ATCC HTB-96) and Vero (ATCC CCL-
440 81) cells were grown in Dulbecco's minimal essential medium (DMEM) with 10% FBS and 1%
441 antibiotic. Human foreskin fibroblast (HFF), JEG-3 and JAR were purchased from the ATCC and
442 cultured as previously described [10, 47]. HEK-Blue IFN-λ reporter cells (hkb-ifnl) were purchased
443 from InvivoGen and cultured according to the manufacturer's instructions. ZIKV (Paraiba/2015,
444 provided by David Watkins, University of Miami) was propagated in Vero cells. Viral titers were
445 determined by fluorescent focus assay as previously described [48] using recombinant anti-double-
446 stranded RNA monoclonal antibody J2 (provided by Abraham Brass, University of Massachusetts)
447 in Vero cells. Infection was determined by qRT-PCR as described below. To assess antiviral activity,
448 U2OS cells were exposed to TO or DO CM, or matched NCM, 24 hr prior to infection with ZIKV
449 Paraiba/2015 for 72hrs. GFP-tagged AD169r (BADrUL131-Y4, a gift from T. Shenk [25]) and
450 mCherry-tagged TB40/E (a gift from N. Moorman [26]) were propagated by infecting HFF cells (MOI
451 = 0.01) followed by incubation for ~14 days until 90-95% of cells showed cytopathic effect. Cells and
452 supernatant were harvested, filtered (0.45-µm), and then concentrated on a 20% sucrose cushion
453 (20,000 rpm) before the virus pellet was resuspended in sterile media before titration. HCMV
454 infection of TOs and DOs was performed using 3-4x10^6 PFU virus per well for 48hrs. For infections,
455 TOs and DOs were plated directly onto 15µL of a Matrigel coating in each well of an 8-well chamber
456 slide (Millicell, EZslide, Millipore) or onto 20µL of Matrigel coating in 24-well plates and cultured for
457 5-7 days prior to infection. After 48hrs, conditioned media was harvested and stored at -80 °C until
458 Luminex profiling and cells were fixed with paraformaldehyde for 15mins before staining for
459 immunofluorescence microscopy, as detailed below.
460
461 **Immunofluorescence microscopy.** TOs and DOs were released from Matrigel domes with 1 mL of
462 cell recovery solution (Corning, 354253) per well without disrupting their 3D architecture, then were
463 fixed in 4%PFA for 30 min at room temperature, followed by 0.5% Triton X-100/PBS to permeabilize

464 for 30 min at 4°C. Organoids were washed and blocked in 5%(v/v) goat serum/0.1%(v/v) Tween-20
465 in PBS for 15 min at room temperature and then incubated with primary antibodies in the above-
466 described blocking solution at 4°C overnight. Organoids were then washed with PBS and then
467 incubated for 1-2 h at room temperature with Alexa Fluor-conjugated secondary antibodies
468 (Invitrogen). Organoids were washed again with PBS and mounted in Vectashield (Vector
469 Laboratories) containing 4′,6-diamidino- 2-phenylindole (DAPI) and were transferred onto
470 microscope slides with large-orifice 200 µL-tips (Fisher Scientific, 02707134). The following
471 antibodies or reagents were used: cytokeratin-19 (Abcam, ab9221), E-cadherin (Invitrogen, PA5-
472 85088), EpCAM (Abcam, ab223582), Mucin 5AC (Abcam, ab3649), SIGLEC6 (Abcam, ab262851),
473 HLA-G (Abcam, ab52454), Ki67 (550609, BD Biosciences), Alexa Fluor 594–conjugated phalloidin
474 (Invitrogen, A12381), Alexa Fluor Plus 488 Goat anti-Mouse IgG secondary antibody (Invitrogen,
475 A32723), Alexa Fluor 594 Goat anti-Mouse IgG secondary antibody (Invitrogen, A11032), Alexa
476 Fluor 488 Goat anti-Rabbit IgG secondary antibody (Invitrogen, A11034), Alexa Fluor 594 Goat anti-
477 Rabbit IgG secondary antibody (Invitrogen, A11037). Images were captured using Zeiss 880
478 Airyscan Fast Inverted confocal microscope and contrast-adjusted in Photoshop or Fiji. For whole
479 Matrigel dome images, scans were performed using a 10x objective on an inverted IX83 Olympus
480 microscopy with a motorized XY-stage (Prior) and tiled images automatically generated by CellSens
481 (Olympus).
482

483 **Immunohistochemistry**

484 Tissue sections were deparaffinized with xylene and rehydrated with decreasing concentrations of
485 ethanol (100%, 95%, 80%), then washed with ddH_20. Antigen retrieval was performed with slides
486 submerged in 10 mM citrate buffer (pH 6.0) and heated in a steamer for 90°C for 20min. Slides were
487 cooled to room temperature and incubated with 6% H_2O_2 in methanol for 30 min. Following washing
488 in 0.1% PBS-T (Phosphate-buffered saline, 0.1% Tween 20), slides were incubated in Avidin
489 blocking solution for 15min, following by subsequent blocking in Biotin blocking solution for 15min

490 (Vector Laboratories, SP-2001). Following washing in 0.1% PBS-T, slides were then incubated with
491 serum-free Protein Block (Abcam, ab156024) for 10min. Sections were incubated with primary
492 antibodies (cytokeratin-19 (Abcam, ab9221) and Ki67 (550609, BD Biosciences) diluted 1:250 in
493 PBS-T overnight in a humidified chamber at 4°C. Next, slides were washed with PBS-T and
494 incubated with secondary antibody (Biotinylated Goat Anti-Rabbit or Mouse IgG, Vector Biolabs BA-
495 1000 and BA-9200) for 30min, washed, and then incubated with avidin/biotin-based peroxidase
496 (Vector Laboratories, Vectastain Elite ABC HRP Kit, PK-6100) for an additional 30min. Following
497 washes in PBT-T, sections were incubated with DAB substrate (Vector Laboratories, SK-4100) for
498 ~5min. Slides were washed with dd$H_2$0 and then counterstained with hematoxylin for 1 min,
499 thoroughly rinsed with H_2O, and incubated in 0.1% sodium bicarbonate in H_2O for 5 mins. Slides
500 were then dehydrated with increasing concentrations of ethanol, cleared with xylene and mounted
501 with Vectamount Permanent Mounting Medium (Vector Laboratories, H-5000). Images were
502 captured on an IX83 inverted microscope (Olympus) using a UC90 color CCD camera (Olympus).
503
504 **RNA extraction, cDNA synthesis and quantitative PCR.** Total RNA was extracted with the Sigma
505 GenElute total mammalian RNA miniprep kit following the manufacturer's instruction and using the
506 supplementary Sigma DNase digestion. RNA quality and concentration were determined using a
507 Nanodrop ND-1000 Spectrophotometer. Total RNA was reverse-transcribed with the iScript cDNA
508 synthesis kit (Bio-Rad) following the manufacturer's instructions. Quantitative PCR was performed
509 using the iQ SYBR Green Supermix (Bio-Rad, 1708882) on a CFX96 Touch Real-Time PCR
510 Detection System (Bio-Rad). Gene expression was determined based on a ΔC_T method normalized
511 to actin. The expression level of C19MC miRNAs hsa-miR-516b-5p, hsa-miR-517a-3p, hsa-miR-
512 525-5p and reference gene RNU6 was quantified by using the MystiCq® MicroRNA® Quantitation
513 System (Millipore Sigma) which includes miRNAs Poly(A) tailing, cDNA synthesis (MIRRT) and
514 miRNA qPCR (MIRRM00). MicroRNAs were first polyadenylated in a poly(A) polymerase reaction,
515 then reverse transcribed using an oligo-dT adapter primer according to the manufacturer's protocol

516 (Sigma-Aldrich, MIRRT). Individual microRNAs (microRNA-516b-5p, microRNA-517a-3p and
517 microRNA-525-5p) were quantified in real-time SYBR® Green RT-qPCR reactions with the specific
518 MystiCq microRNA qPCR Assay Primer (MIRAP00475, MIRAP00477 and MIRAP00512) and the
519 MystiCq Universal PCR Primer (MIRUP). Cq reading were normalized to the RNU6 internal reference
520 by the $2^{-\Delta Cq}$ method.
521
522 **RNAseq analysis**. For RNAseq analysis, RNA was isolated from organoids as described above.
523 Purified Total RNA was verified by Thermo scientific Nanodrop one. The libraries were prepared by
524 the Duke Center for Genomic and Computational Biology (GCB) using the Tru-Seq stranded total
525 RNA prep kit (Illumina). Sequencing was performed on the NovaSeq 6000 by using 150-bp paired-
526 end sequencing. The reads were aligned to the human reference genome (GRCh38) using QIAGEN
527 CLC Genomics (v20). DESeq2 [49] was used to normalized count data and to do the differential
528 gene expression analysis with a significance cutoff of 0.01 and a fold change cutoff of $\log_2(2)$.
529 Heatmaps and hierarchical clustering was performed in R using pheatmap package in R and were
530 based on RPKM (reads per kilobase million). Files associated with RNA-seq studies have been
531 deposited into Sequence Read Archive under accession number SRA. Data from PHT cells
532 (accession SRP067137 and SRP109039) [10, 11, 50]. Principal component analyses were
533 performed using pcaExplorer in R [51] or GraphPad Prism. Volcano plots were generated using the
534 EnhancedVolcano package in R [52] or in Graphpad Prism.
535
536 **Luminex assays**. All sample processing was performed in duplicates and each experiment was
537 performed with at least three biological replicates. Luminex assays were performed using the
538 following kits according to the manufacturer's instructions: Bio-Plex Pro Human Inflammation Panel
539 1, 37-Plex kit (171AL001M; Bio-Rad) Bio-Plex Human Chemokine Panel, 40-plex (171AK99MR2;
540 Bio-Rad), Bio-Plex Pro Human Cytokine Screening Panel, 48-Plex kit (12007283; Bio-Rad), hCG
541 Human ProcartaPlex Simplex Kit (EPX010-12388-901) and CA125 (Mucin-16) Human ProcartaPlex

542 Simplex Kit (EPX010-12437-901). Plates were read on MAGPIX (EMD Millipore) or Bio-Plex 200
543 (Bio-Rad) Luminex machines and analyzed using xPONENT (EMD Millipore) or Bio-Plex (Biorad)
544 software.
545
546 **IFN-λ activity reporter assay.** For IFN-λ activity detection from CM, HEK-Blue IFN-λ reporter cells
547 were used according to the manufacture's protocol. Briefly, IFN-λ reporter cells were plated into a
548 96-well plate, then CM was added and incubated at 37 °C for 24 hr. Supernatants (20 µl) were
549 collected and then transferred into a 96-well plate and activity measured using QUANTI-Blue
550 Solution (InvivoGen, rep-qbs) after incubating at 37 °C for 2 hr using a spectrophotometer at 655 nm.
551 Each CM preparation was run in triplicate.
552
553 **Poly(I:C) treatment.** For Poly (I:C) treatment, TOs or DOs were incubated with 10 µg/mL Poly (I:C)
554 diluted in organoid complete growth media for ~24 h, then supernatant was collected for Luminex-
555 based multianalyte profiling or RNA isolated as described for qRT-PCR or RNASeq.
556
557 **Statistics and reproducibility.** All experiments reported in this study have been reproduced using
558 independent samples (tissues and organoids) from multiple donors. All statistical analyses were
559 performed using Prism software (GraphPad Software). Data are presented as mean ± SD, unless
560 otherwise stated. Statistical significance was determined as described in the figure legends.
561 Parametric tests were applied when data were distributed normally based on D'Agostino-Pearson
562 analyses; otherwise, nonparametric tests were applied. P values <0.05 were considered statistically
563 significant, with specific P values noted in the figure legends.
564
565 **Author contributions** LY designed and performed experiments and participated in manuscript
566 review and writing, ECS designed and performed experiments and participated in manuscript review
567 and writing, CO performed experiments and participated in manuscript review and writing, JG

provided placental tissue and participated in manuscript review and writing, CM performed tissue dissections and participated in manuscript review and writing, SP designed experiments and participated in manuscript review and writing, and CC designed and performed experiments, participated in manuscript review and writing, and secured funding.

Acknowledgements

We thank Jon Boyle (University of Pittsburgh) for careful review of the manuscript and Alexandra Wells for assistance with bioinformatics. This project was supported by NIH AI145828 (C.B.C.).

Literature Cited

1. Megli CJ, Coyne CB. Infections at the maternal-fetal interface: an overview of pathogenesis and defence. Nat Rev Microbiol. 2021. Epub 20210825. doi: 10.1038/s41579-021-00610-y. PubMed PMID: 34433930; PubMed Central PMCID: PMCPMC8386341.

2. Semmes EC, Coyne CB. Innate immune defenses at the maternal-fetal interface. Curr Opin Immunol. 2021;74:60-7. Epub 20211109. doi: 10.1016/j.coi.2021.10.007. PubMed PMID: 34768027.

3. McDonagh S, Maidji E, Chang HT, Pereira L. Patterns of human cytomegalovirus infection in term placentas: a preliminary analysis. J Clin Virol. 2006;35(2):210-5. Epub 2006/01/03. doi: 10.1016/j.jcv.2005.08.011. PubMed PMID: 16386950.

4. Weisblum Y, Panet A, Zakay-Rones Z, Haimov-Kochman R, Goldman-Wohl D, Ariel I, et al. Modeling of human cytomegalovirus maternal-fetal transmission in a novel decidual organ culture. J Virol. 2011;85(24):13204-13. Epub 2011/10/07. doi: 10.1128/JVI.05749-11. PubMed PMID: 21976654; PubMed Central PMCID: PMCPMC3233115.

5. Pereira L, Maidji E, McDonagh S, Genbacev O, Fisher S. Human cytomegalovirus transmission from the uterus to the placenta correlates with the presence of pathogenic bacteria and maternal immunity. J Virol. 2003;77(24):13301-14. Epub 2003/12/04. doi: 10.1128/jvi.77.24.13301-13314.2003. PubMed PMID: 14645586; PubMed Central PMCID: PMCPMC296088.

6. Weisblum Y, Oiknine-Djian E, Vorontsov OM, Haimov-Kochman R, Zakay-Rones Z, Meir K, et al. Zika Virus Infects Early- and Midgestation Human Maternal Decidual Tissues, Inducing Distinct Innate Tissue Responses in the Maternal-Fetal Interface. J Virol. 2017;91(4). Epub 2016/12/16. doi: 10.1128/JVI.01905-16. PubMed PMID: 27974560; PubMed Central PMCID: PMCPMC5286880.

7. Guzeloglu-Kayisli O, Guo X, Tang Z, Semerci N, Ozmen A, Larsen K, et al. Zika Virus-Infected Decidual Cells Elicit a Gestational Age-Dependent Innate Immune Response and Exaggerate Trophoblast Zika Permissiveness: Implication for Vertical Transmission. J Immunol. 2020;205(11):3083-94. Epub 2020/11/04. doi: 10.4049/jimmunol.2000713. PubMed PMID: 33139490.

8. Platt DJ, Smith AM, Arora N, Diamond MS, Coyne CB, Miner JJ. Zika virus-related neurotropic flaviviruses infect human placental explants and cause fetal demise in mice. Sci Transl Med. 2018;10(426). Epub 2018/02/02. doi: 10.1126/scitranslmed.aao7090. PubMed PMID: 29386359; PubMed Central PMCID: PMCPMC6136894.

9. Rizzuto G, Tagliani E, Manandhar P, Erlebacher A, Bakardjiev AI. Limited Colonization Undermined by Inadequate Early Immune Responses Defines the Dynamics of Decidual Listeriosis. Infect Immun. 2017;85(8). Epub 2017/05/17. doi: 10.1128/IAI.00153-17. PubMed PMID: 28507070; PubMed Central PMCID: PMCPMC5520438.

10. Bayer A, Lennemann NJ, Ouyang Y, Bramley JC, Morosky S, Marques ET, Jr., et al. Type III Interferons Produced by Human Placental Trophoblasts Confer Protection against Zika Virus

631 Infection. Cell Host Microbe. 2016;19(5):705-12. Epub 20160405. doi: 10.1016/j.chom.2016.03.008.
632 PubMed PMID: 27066743; PubMed Central PMCID: PMCPMC4866896.

633 11. Corry J, Arora N, Good CA, Sadovsky Y, Coyne CB. Organotypic models of type III interferon-
634 mediated protection from Zika virus infections at the maternal-fetal interface. Proc Natl Acad Sci U
635 S A. 2017;114(35):9433-8. Epub 2017/08/09. doi: 10.1073/pnas.1707513114. PubMed PMID:
636 28784796; PubMed Central PMCID: PMCPMC5584447.

637 12. Lazear HM, Schoggins JW, Diamond MS. Shared and Distinct Functions of Type I and Type
638 III Interferons. Immunity. 2019;50(4):907-23. Epub 2019/04/18. doi: 10.1016/j.immuni.2019.03.025.
639 PubMed PMID: 30995506; PubMed Central PMCID: PMCPMC6839410.

640 13. Wells AI, Coyne CB. Type III Interferons in Antiviral Defenses at Barrier Surfaces. Trends
641 Immunol. 2018;39(10):848-58. Epub 2018/09/17. doi: 10.1016/j.it.2018.08.008. PubMed PMID:
642 30219309; PubMed Central PMCID: PMCPMC6179363.

643 14. Roark HK, Jenks JA, Permar SR, Schleiss MR. Animal Models of Congenital
644 Cytomegalovirus Transmission: Implications for Vaccine Development. J Infect Dis. 2020;221(Suppl
645 1):S60-S73. doi: 10.1093/infdis/jiz484. PubMed PMID: 32134481; PubMed Central PMCID:
646 PMCPMC7057791.

647 15. Njue A, Coyne C, Margulis AV, Wang D, Marks MA, Russell K, et al. The Role of Congenital
648 Cytomegalovirus Infection in Adverse Birth Outcomes: A Review of the Potential Mechanisms.
649 Viruses. 2020;13(1). Epub 2020/12/31. doi: 10.3390/v13010020. PubMed PMID: 33374185;
650 PubMed Central PMCID: PMCPMC7823935.

651 16. Fisher S, Genbacev O, Maidji E, Pereira L. Human cytomegalovirus infection of placental
652 cytotrophoblasts in vitro and in utero: implications for transmission and pathogenesis. Journal of
653 virology. 2000;74(15):6808-20. Epub 2000/07/11. doi: 10.1128/jvi.74.15.6808-6820.2000. PubMed
654 PMID: 10888620; PubMed Central PMCID: PMCPMC112198.

655 17. Turco MY, Gardner L, Kay RG, Hamilton RS, Prater M, Hollinshead MS, et al. Trophoblast
656 organoids as a model for maternal-fetal interactions during human placentation. Nature.
657 2018;564(7735):263-7. Epub 2018/11/30. doi: 10.1038/s41586-018-0753-3. PubMed PMID:
658 30487605; PubMed Central PMCID: PMCPMC7220805.

659 18. Turco MY, Gardner L, Hughes J, Cindrova-Davies T, Gomez MJ, Farrell L, et al. Long-term,
660 hormone-responsive organoid cultures of human endometrium in a chemically defined medium. Nat
661 Cell Biol. 2017;19(5):568-77. Epub 2017/04/11. doi: 10.1038/ncb3516. PubMed PMID: 28394884;
662 PubMed Central PMCID: PMCPMC5410172.

663 19. Sheridan MA, Fernando RC, Gardner L, Hollinshead MS, Burton GJ, Moffett A, et al.
664 Establishment and differentiation of long-term trophoblast organoid cultures from the human
665 placenta. Nat Protoc. 2020;15(10):3441-63. Epub 2020/09/11. doi: 10.1038/s41596-020-0381-x.
666 PubMed PMID: 32908314.

667 20. Okae H, Toh H, Sato T, Hiura H, Takahashi S, Shirane K, et al. Derivation of Human
668 Trophoblast Stem Cells. Cell Stem Cell. 2018;22(1):50-63 e6. Epub 2017/12/19. doi:
669 10.1016/j.stem.2017.11.004. PubMed PMID: 29249463.

670 21. Haider S, Meinhardt G, Saleh L, Kunihs V, Gamperl M, Kaindl U, et al. Self-Renewing
671 Trophoblast Organoids Recapitulate the Developmental Program of the Early Human Placenta.
672 Stem Cell Reports. 2018;11(2):537-51. Epub 2018/08/07. doi: 10.1016/j.stemcr.2018.07.004.
673 PubMed PMID: 30078556; PubMed Central PMCID: PMCPMC6092984.

674 22. Marinic M, Rana S, Lynch VJ. Derivation of endometrial gland organoids from term placenta.
675 Placenta. 2020;101:75-9. Epub 2020/09/17. doi: 10.1016/j.placenta.2020.08.017. PubMed PMID:
676 32937244.

677 23. Mouillet JF, Ouyang Y, Coyne CB, Sadovsky Y. MicroRNAs in placental health and disease.
678 Am J Obstet Gynecol. 2015;213(4 Suppl):S163-72. Epub 2015/10/03. doi:
679 10.1016/j.ajog.2015.05.057. PubMed PMID: 26428496; PubMed Central PMCID:
680 PMCPMC4592520.

681 24. Megli C, Morosky S, Rajasundaram D, Coyne CB. Inflammasome signaling in human
682 placental trophoblasts regulates immune defense against Listeria monocytogenes infection. J Exp
683 Med. 2021;218(1). Epub 2020/09/26. doi: 10.1084/jem.20200649. PubMed PMID: 32976558.

684 25. Wang D, Shenk T. Human cytomegalovirus UL131 open reading frame is required for
685 epithelial cell tropism. Journal of virology. 2005;79(16):10330-8. Epub 2005/07/30. doi:
686 10.1128/jvi.79.16.10330-10338.2005. PubMed PMID: 16051825; PubMed Central PMCID:
687 PMCPMC1182637.

688 26. O'Connor CM, Shenk T. Human cytomegalovirus pUS27 G protein-coupled receptor
689 homologue is required for efficient spread by the extracellular route but not for direct cell-to-cell
690 spread. Journal of virology. 2011;85(8):3700-7. Epub 2011/02/11. doi: 10.1128/jvi.02442-10.
691 PubMed PMID: 21307184; PubMed Central PMCID: PMCPMC3126124.

692 27. Breviario F, d'Aniello EM, Golay J, Peri G, Bottazzi B, Bairoch A, et al. Interleukin-1-inducible
693 genes in endothelial cells. Cloning of a new gene related to C-reactive protein and serum amyloid P
694 component. J Biol Chem. 1992;267(31):22190-7. PubMed PMID: 1429570.

695 28. Pass RF, Anderson B. Mother-to-Child Transmission of Cytomegalovirus and Prevention of
696 Congenital Infection. J Pediatric Infect Dis Soc. 2014;3 Suppl 1:S2-6. doi: 10.1093/jpids/piu069.
697 PubMed PMID: 25232473; PubMed Central PMCID: PMCPMC4164178.

698 29. Ander SE, Rudzki EN, Arora N, Sadovsky Y, Coyne CB, Boyle JP. Human Placental
699 Syncytiotrophoblasts Restrict Toxoplasma gondii Attachment and Replication and Respond to
700 Infection by Producing Immunomodulatory Chemokines. mBio. 2018;9(1). Epub 2018/01/11. doi:
701 10.1128/mBio.01678-17. PubMed PMID: 29317509; PubMed Central PMCID: PMCPMC5760739.

30. Liu J, Hao S, Chen X, Zhao H, Du L, Ren H, et al. Human placental trophoblast cells contribute to maternal-fetal tolerance through expressing IL-35 and mediating iTR35 conversion. Nat Commun. 2019;10(1):4601. Epub 2019/10/12. doi: 10.1038/s41467-019-12484-z. PubMed PMID: 31601798; PubMed Central PMCID: PMCPMC6787064.

31. Vassiliadis S, Ranella A, Papadimitriou L, Makrygiannakis A, Athanassakis I. Serum levels of pro- and anti-inflammatory cytokines in non-pregnant women, during pregnancy, labour and abortion. Mediators Inflamm. 1998;7(2):69-72. Epub 1998/12/04. doi: 10.1080/09629359891199. PubMed PMID: 9836491; PubMed Central PMCID: PMCPMC1781827.

32. Benyo DF, Smarason A, Redman CW, Sims C, Conrad KP. Expression of inflammatory cytokines in placentas from women with preeclampsia. J Clin Endocrinol Metab. 2001;86(6):2505-12. Epub 2001/06/09. doi: 10.1210/jcem.86.6.7585. PubMed PMID: 11397847.

33. Lash GE, Ernerudh J. Decidual cytokines and pregnancy complications: focus on spontaneous miscarriage. J Reprod Immunol. 2015;108:83-9. Epub 2015/03/17. doi: 10.1016/j.jri.2015.02.003. PubMed PMID: 25771398.

34. von Rango U, Classen-Linke I, Raven G, Bocken F, Beier HM. Cytokine microenvironments in human first trimester decidua are dependent on trophoblast cells. Fertil Steril. 2003;79(5):1176-86. Epub 2003/05/10. doi: 10.1016/s0015-0282(02)04829-x. PubMed PMID: 12738514.

35. Alam SM, Konno T, Sahgal N, Lu L, Soares MJ. Decidual cells produce a heparin-binding prolactin family cytokine with putative intrauterine regulatory actions. J Biol Chem. 2008;283(27):18957-68. Epub 2008/05/10. doi: 10.1074/jbc.M801826200. PubMed PMID: 18467328; PubMed Central PMCID: PMCPMC2441551.

36. Denison FC, Kelly RW, Calder AA, Riley SC. Cytokine secretion by human fetal membranes, decidua and placenta at term. Hum Reprod. 1998;13(12):3560-5. Epub 1999/01/14. doi: 10.1093/humrep/13.12.3560. PubMed PMID: 9886550.

37. Laham N, Brennecke SP, Rice GE. Interleukin-8 release from human gestational tissue explants: the effects of lipopolysaccharide and cytokines. Biol Reprod. 1997;57(3):616-20. Epub 1997/09/01. doi: 10.1095/biolreprod57.3.616. PubMed PMID: 9282999.

38. Pitman H, Innes BA, Robson SC, Bulmer JN, Lash GE. Altered expression of interleukin-6, interleukin-8 and their receptors in decidua of women with sporadic miscarriage. Hum Reprod. 2013;28(8):2075-86. Epub 2013/06/07. doi: 10.1093/humrep/det233. PubMed PMID: 23739222.

39. Qiu X, Zhu L, Pollard JW. Colony-stimulating factor-1-dependent macrophage functions regulate the maternal decidua immune responses against Listeria monocytogenes infections during early gestation in mice. Infect Immun. 2009;77(1):85-97. Epub 2008/10/15. doi: 10.1128/IAI.01022-08. PubMed PMID: 18852237; PubMed Central PMCID: PMCPMC2612255.

40. Barber EM, Fazzari M, Pollard JW. Th1 cytokines are essential for placental immunity to Listeria monocytogenes. Infect Immun. 2005;73(10):6322-31. Epub 2005/09/24. doi:

738 10.1128/IAI.73.10.6322-6331.2005. PubMed PMID: 16177303; PubMed Central PMCID:
739 PMCPMC1230899.

740 41. Rudzki EN, Ander SE, Coombs RS, Alrubaye HS, Cabo LF, Blank ML, et al. Toxoplasma
741 gondii GRA28 Is Required for Placenta-Specific Induction of the Regulatory Chemokine CCL22 in
742 Human and Mouse. mBio. 2021:e0159121. Epub 20211116. doi: 10.1128/mBio.01591-21. PubMed
743 PMID: 34781732.

744 42. Freier CP, Kuhn C, Rapp M, Endres S, Mayr D, Friese K, et al. Expression of CCL22 and
745 Infiltration by Regulatory T Cells are Increased in the Decidua of Human Miscarriage Placentas. Am
746 J Reprod Immunol. 2015;74(3):216-27. Epub 20150428. doi: 10.1111/aji.12399. PubMed PMID:
747 25922986.

748 43. Weisblum Y, Panet A, Zakay-Rones Z, Vitenshtein A, Haimov-Kochman R, Goldman-Wohl
749 D, et al. Human cytomegalovirus induces a distinct innate immune response in the maternal-fetal
750 interface. Virology. 2015;485:289-96. Epub 2015/09/01. doi: 10.1016/j.virol.2015.06.023. PubMed
751 PMID: 26318261.

752 44. Scott GM, Chow SS, Craig ME, Pang CN, Hall B, Wilkins MR, et al. Cytomegalovirus infection
753 during pregnancy with maternofetal transmission induces a proinflammatory cytokine bias in
754 placenta and amniotic fluid. The Journal of infectious diseases. 2012;205(8):1305-10. Epub
755 2012/03/03. doi: 10.1093/infdis/jis186. PubMed PMID: 22383678.

756 45. Kovács IJ, Hegedűs K, Pál A, Pusztai R. Production of Proinflammatory Cytokines by
757 Syncytiotrophoblasts Infected with Human Cytomegalovirus Isolates. Placenta. 2007;28(7):620-3.
758 doi: https://doi.org/10.1016/j.placenta.2006.09.008.

759 46. Turco M, Gardner, L., Koo, B., Moffett, A., & Burton, G. Derivation and long-term expansion
760 of human endometrial and decidual organoids. Protocol Exchange. 2017. doi:
761 10.1038/protex.2017.030.

762 47. Drummond CG, Nickerson CA, Coyne CB. A Three-Dimensional Cell Culture Model To Study
763 Enterovirus Infection of Polarized Intestinal Epithelial Cells. mSphere. 2016;1(1). Epub 2016/06/16.
764 doi: 10.1128/mSphere.00030-15. PubMed PMID: 27303677; PubMed Central PMCID:
765 PMCPMC4863623.

766 48. Payne AF, Binduga-Gajewska I, Kauffman EB, Kramer LD. Quantitation of flaviviruses by
767 fluorescent focus assay. J Virol Methods. 2006;134(1-2):183-9. Epub 2006/03/03. doi:
768 10.1016/j.jviromet.2006.01.003. PubMed PMID: 16510196.

769 49. Love MI, Huber W, Anders S. Moderated estimation of fold change and dispersion for RNA-
770 seq data with DESeq2. Genome Biol. 2014;15(12):550. Epub 2014/12/18. doi: 10.1186/s13059-014-
771 0550-8. PubMed PMID: 25516281; PubMed Central PMCID: PMCPMC4302049.

772 50. Van Twisk D, Murphy SP, Thakar J. Optimized logic rules reveal interferon-gamma-induced
773 modes regulated by histone deacetylases and protein tyrosine phosphatases. Immunology.

774 2017;151(1):71-80. Epub 2017/01/06. doi: 10.1111/imm.12707. PubMed PMID: 28054346; PubMed
775 Central PMCID: PMCPMC5382347.

776 51. Marini F, Binder H. Available from:
777 https://www.bioconductor.org/packages/release/bioc/vignettes/pcaExplorer/inst/doc/pcaExplorer.ht
778 ml.

779 52. Blighe K, Rana S, Lewis M. EnhancedVolcano: Publication-ready volcano plots with
780 enhanced colouring and labeling. R package version 1.10.0 2021. Available from:
781 https://github.com/kevinblighe/EnhancedVolcano.
782

783

784

785

786

787

788

789

790

791

792

793

794

795

796

797

798

799

800

801

802 **Figure1**

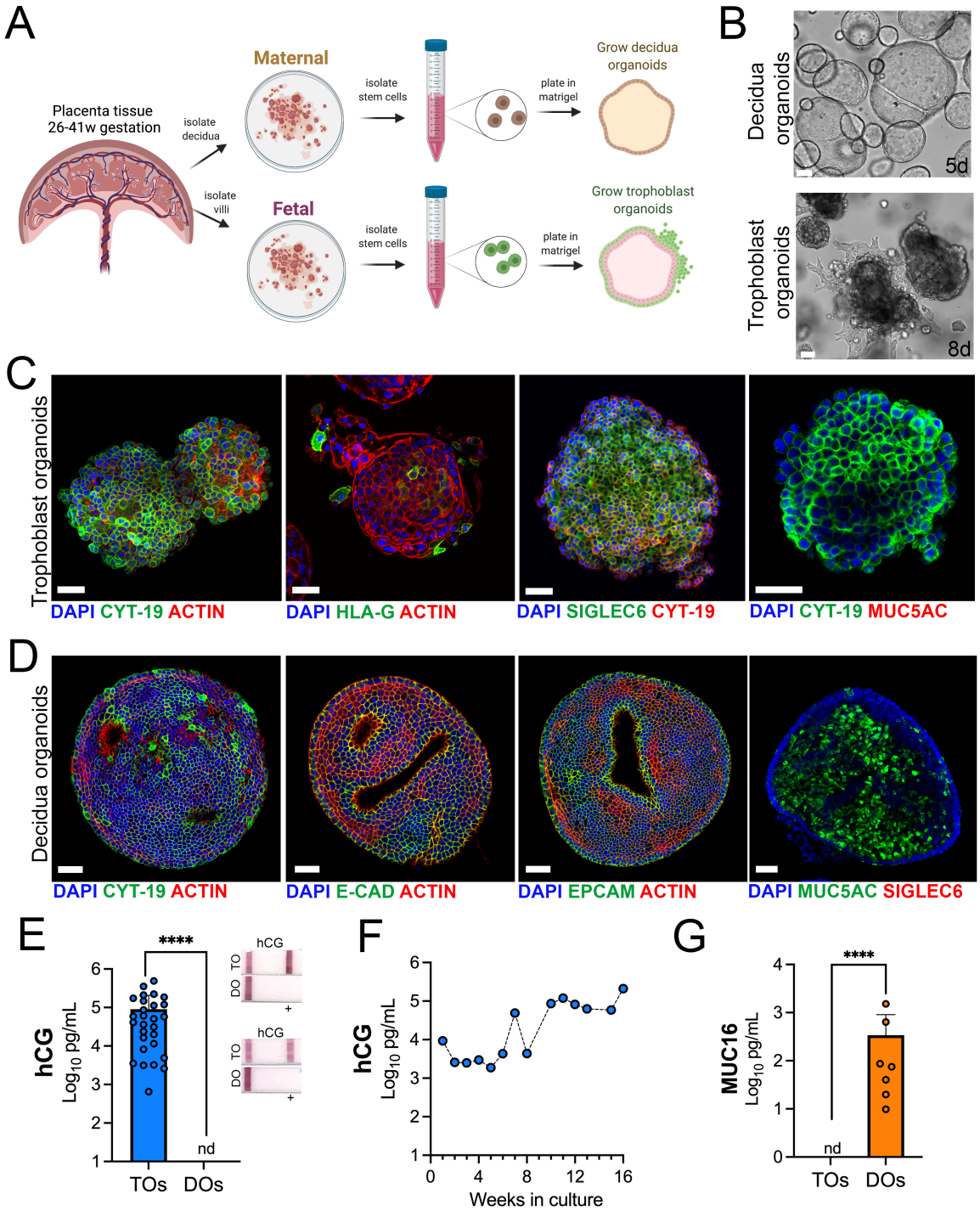

803
804
805 **Figure 1. Long-term three-dimensional organoids cultures can be established from human**
806 **mid- and late-gestation placental tissue. (A)** Schematic representation of the derivation of
807 trophoblast organoids (TOs) and decidual organoids (DOs) from mid-to-late gestation placental
808 tissue. **(B)** Representative bright-field images of TOs and DOs after passaging in complete growth

medium TOM and ExM, respectively at 5 days (DO, top) or 8 days (TO, bottom) post-passaging. Scale bar, 50 μm. **(C)** Confocal microscopy in TOs immunostained for (from left) cytokeratin-19, HLA-G, SIGLEC-6, cytokeratin-19 (in green) and actin, cytokeratin-19, or MUC5AC (in red). DAPI-stained nuclei are shown in blue. Individual channels are shown in Supplemental Figure 1D. Scale bar, 50 μm. **(D)** Confocal microscopy in DOs immunostained for (from left) cytokeratin-19, E-cadherin (E-cad), EpCAM, or MUC5AC (in green) and actin or SIGLEC6 (in red). DAPI-stained nuclei are shown in blue. Individual channels are shown in Supplemental Figure 1D. Scale bar, 50 μm. **(E)** Levels of hCG in conditioned medium (CM) isolated from TOs (blue) or DOs (orange) as determined by Luminex. At right, over the counter (OTC) pregnancy tests for hCG in two matched TO and DO lines. **(F)** Levels of hCG in CM isolated from TOs throughout a 16-week culture period as determined by Luminex. **(G)** Levels of secreted Mucin-16 (MUC16) in CM isolated from TOs (light blue) or DOs (orange) as determined by Luminex assays. In (E) and (G) each symbol represents an individual CM preparation and significance was determined by Mann-Whitney U test. ****, $P < 0.0001$ and nd, not detected.

857 **Figure 2**
858

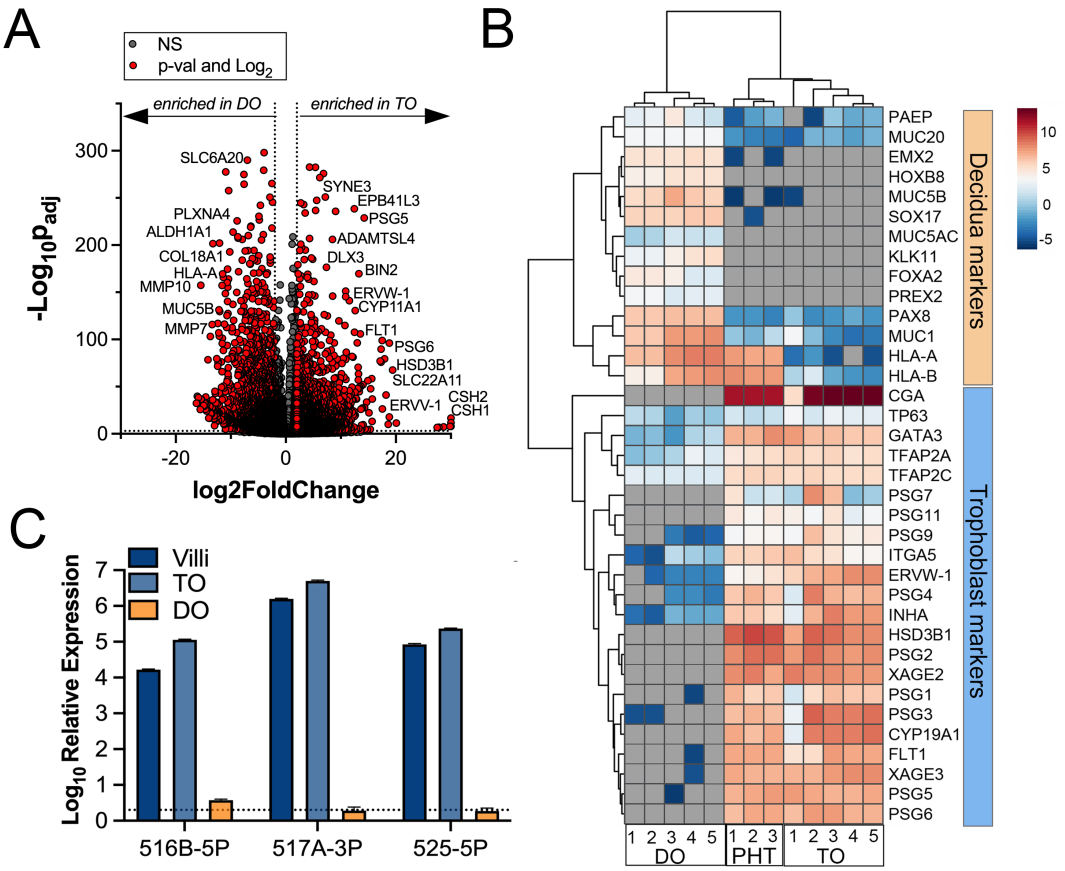

859
860 **Figure 2. Whole genome transcriptional profiling of trophoblast and decidua organoids. (A)**
861 Volcano plot demonstrating differentially expressed transcripts in trophoblast organoids (TOs) or
862 decidua organoids (DOs) as assessed by DeSeq2 analysis. Grey circles represent genes whose
863 expression was not significantly changed and red denotes transcripts significantly enriched in TOs
864 (right) or DOs (left) (significance was set at $p<0.01$ and log2 fold-change of +/- 2). **(B)** Heatmap
865 (based on log2 RPKM values) of transcripts expressed in DOs, TOs, or primary human trophoblasts
866 (PHT) cells that are associated with markers of trophoblasts (top, blue) or the decidua (bottom,
867 orange). Key at right. Red indicates high levels of expression, blue indicates low levels of expression,
868 and grey indicates no reads detected. Hierarchical clustering is shown on left**. (C)** Expression of
869 three members of the C19MC family (miR-516-5p, 517A-3p, and 525-5p) in TOs (light blue) and DOs
870 (orange), or in chorionic villi (dark blue) isolated from human placentas.
871
872
873
874
875
876
877
878
879

Figure 3

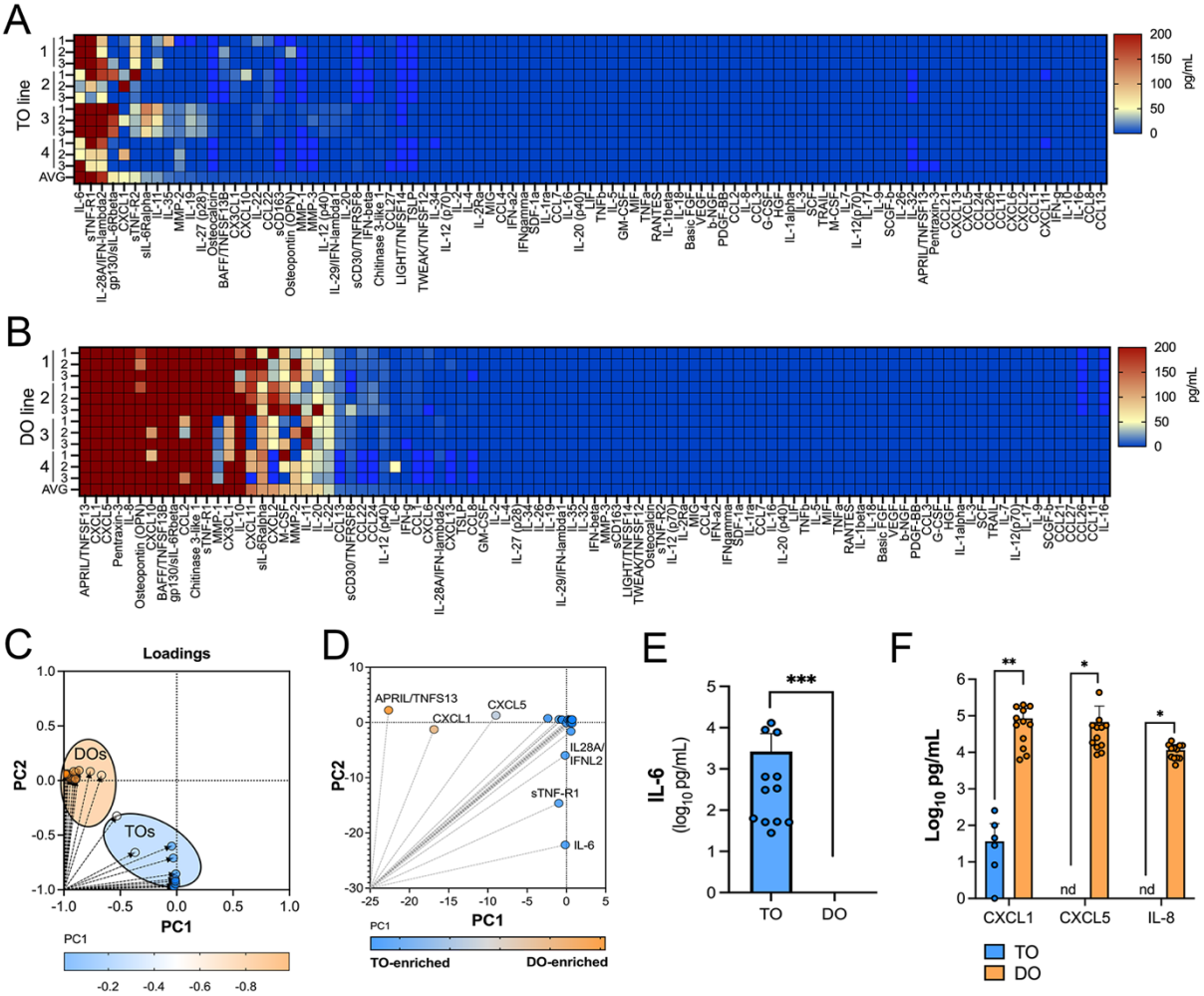

Figure 3. Basal cytokine and chemokine secretion profiles from matched trophoblast and decidua organoids. (A, B) Heatmap of twelve conditioned medium (CM) preparations generated from four established TO (A) and DO (B) lines analyzed by Luminex-based multianalyte profiling for the indicated cytokines, chemokines, and growth factors (at bottom). Scale is shown at right. **(C, D)** Principal component analysis of Luminex data shown in panels A and B indicates that the basal secretion between TOs and DOs is unique (C) and identifies the factors that contribute to these differences (D). **(E)** Basal secretion of IL-6 in TOs, but not DOs, as assessed by Luminex. **(F)** Basal secretion of CXCL1, CXCL5, and IL-8 in CM from TOs (in blue) or DOs (in orange). In (E) and (F) each symbol represents an individual CM preparation and significance was determined by Mann-Whitney U test (E) or Two-way Anova with Šídák's multiple comparisons tests (F). *** $P < 0.001$, ** $P<0.01$, * $P<0.05$.

Figure 4

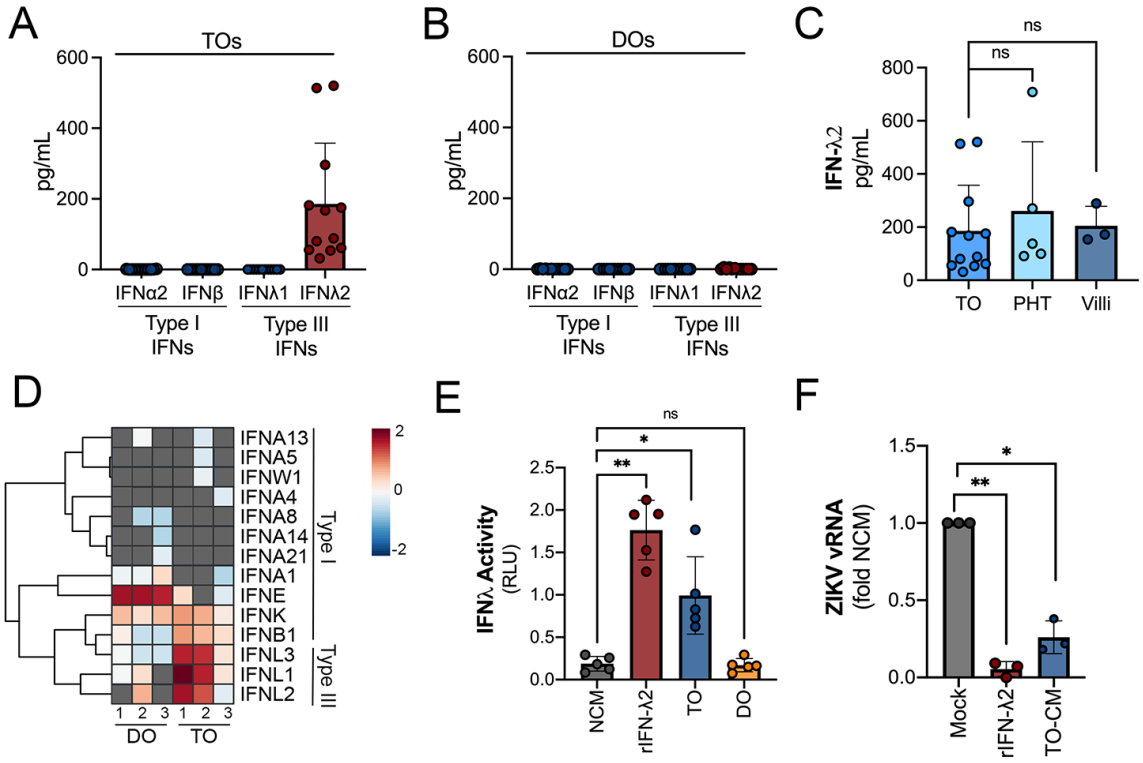

Figure 4. Trophoblast organoids secrete high levels of antiviral IFN-λ2. **(A, B)** Comparison of the levels of the type I IFNs IFN-α2 and IFN-β and type III IFNs IFN-λ1 and IFN-λ2 in conditioned medium (CM) isolated from TOs (A) or DOs (B). **(C)** Comparison of the levels of IFN-λ2 in CM isolated from TOs, matched villous tissue, or in primary human trophoblasts (PHTs). **(D)** Heatmap (based on log2 RPKM values) of transcripts associated with type I (top) or III (bottom) IFNs in TOs or DOs. Key at right. Red indicates high levels of expression, blue indicates low levels of expression, and grey indicates no reads detected. **(E)** IFN-λ activity of CM isolated from TOs (blue) and DOs (orange) as assessed using an IFN-λ reporter 293T cells line. NCM (non-conditioned medium, grey) was as negative control, NCM supplemented with recombinant human IFN-λ2 (100ng) was used as a positive control (red). **(F)** Human osteosarcoma U2OS cells were treated with CM isolated from TOs (blue) or with recombinant IFN-λ2 (100ng) for 24hrs and then infected with ZIKV for 24hrs (in the presence of CM). Level of ZIKV replication was assessed by viral RNA as determined by qPCR. Data are shown as fold change from NCM and from at least three independent CM preparations. Significance was determined by Mann-Whitney U test or by Kruskal Wallace U test with multiple comparisons. *, $P < 0.05$; **, $P < 0.01$; ns, not significant. In A-C, E-F, each symbol represents unique CM preparations.

Figure 5

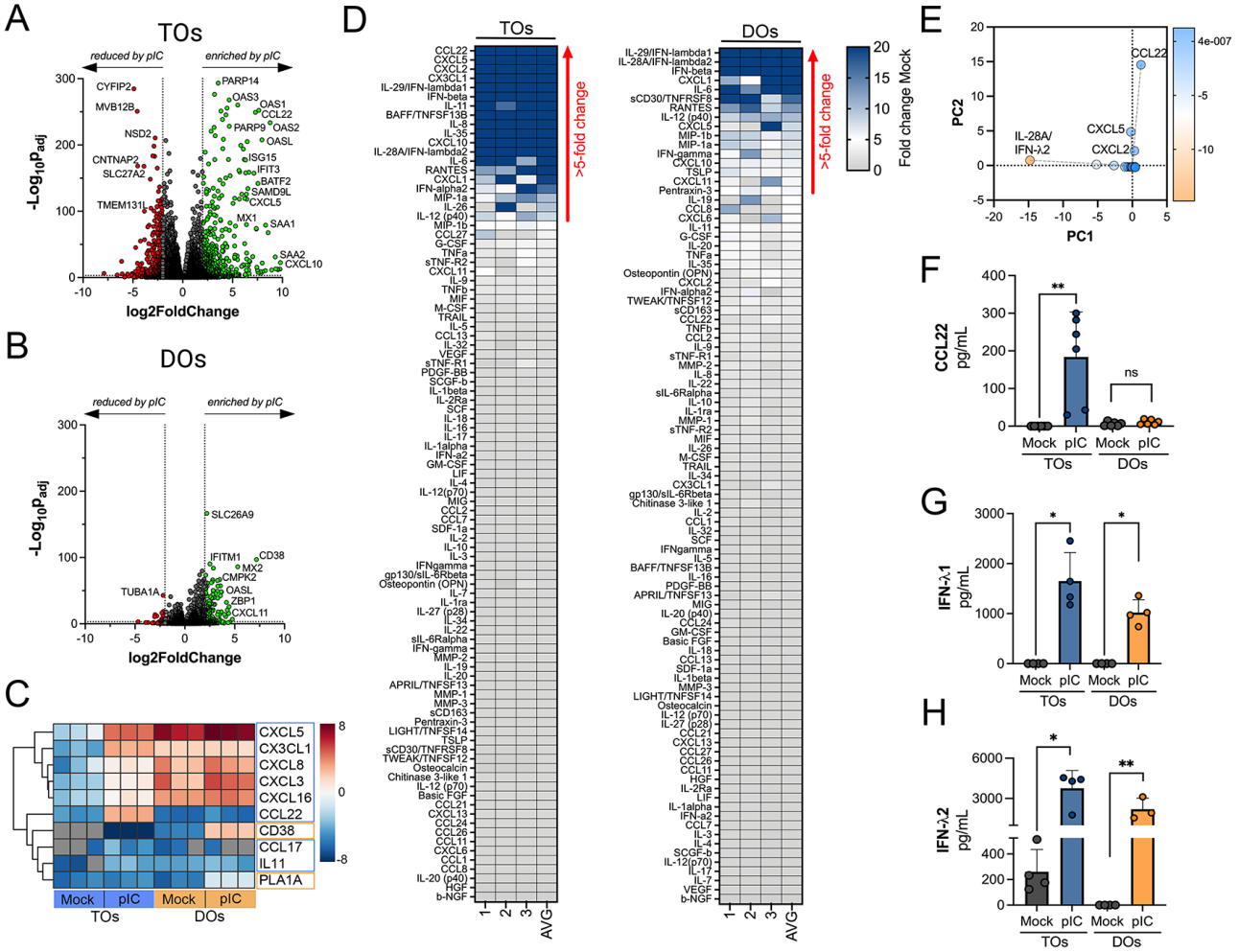

Figure 5. Differential cytokine and chemokine release in TOs and DOs treated with poly I:C. (A, B) Volcano plots demonstrating differentially expressed transcripts in trophoblast organoids (TOs, A) or decidua organoids (DOs, B) treated with poly I:C as assessed by DeSeq2 analysis. Grey circles represent genes whose expression was not significantly changed and green denotes transcripts significantly induced by poly I:C treatment whereas red denotes transcripts significantly reduced by poly I:C treatment. Significance was set at p<0.01 and log2 fold-change of +/- 2. **(C)** Heatmap (based on log2 RPKM values) of select transcripts induced uniquely by poly I:C treatment of TOs (blue boxes) or DOs (orange boxes). Key at right. Red indicates high levels of expression, blue indicates low levels of expression, and grey indicates no reads detected. Hierarchical clustering is on the left. **(D)** Heatmaps demonstrating the induction of factors at left (shown as fold change from mock-treated controls) from TOs (left panel) and DOs (right panel) treated with 10μg poly (I:C) and analyzed by multiplex Luminex-based profiling for 105 cytokines, chemokines, and other factors. AVG denotes the average change in concentration of factors over conditioned medium (CM) isolated from three individual preparations. Dark blue denotes significantly induced factors compared with untreated controls. Gray or white denotes little to no change (scale at top right). The red arrow demonstrates factors with induction greater than five-fold change observed in the average of

separate experiments. Data are from three individual CM preparations from at least three unique matched organoid lines. **(E)** Principal component analysis of Luminex data shown in left panels identify factors differentially induced by poly I:C treatment of TOs and DOs. **(F-H)** Levels of CCL22 (F), IFN-λ1 (G), and IFN-λ2 (H) in CM isolated from poly I:C-treated TOs (blue) or DOs (orange) or in mock-treated controls (grey). In F-H, each symbol represents individual CM preparations. In F-H significance was determined using a Mann-Whitney U test. **, $P < 0.01$, *, $P < 0.05$; ns, not significant**.**

Figure 6

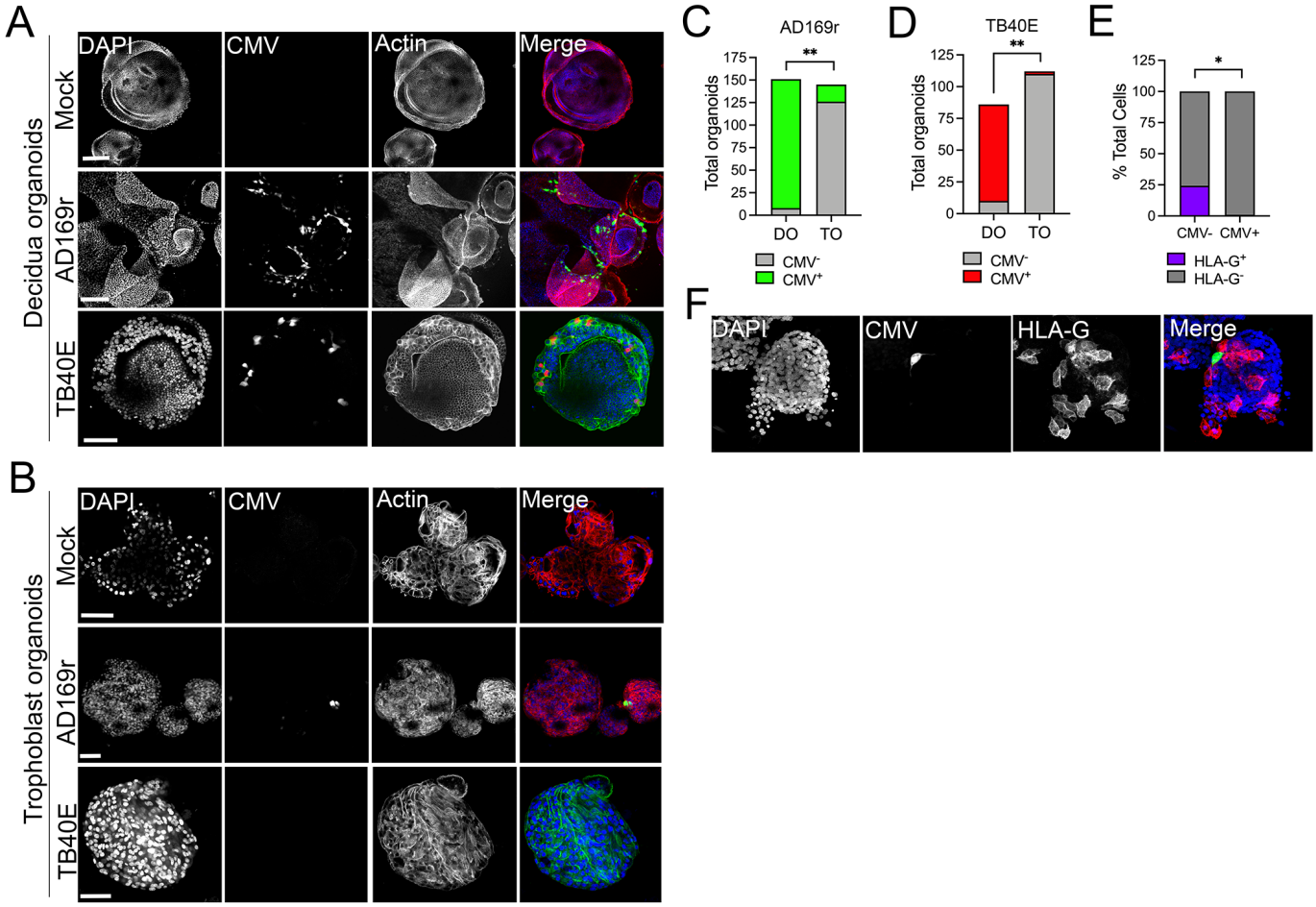

Figure 6. Differential susceptibility of TOs and DOs to HCMV infection. (A, B) Representative confocal micrographs of DOs (A) or TOs (B) infected with human CMV (HCMV) strains EGFP-tagged AD169r and mCherry-tagged TB40E for ~48hrs. Mock infected shown in top row of A and B. Infected cells are positive for EGFP (AD169r, middle row) or mCherry (TB40E, bottom row). Organoids were stained for actin (red in mock- and AD169r-infected or green in TB40E infected). DAPI-stained nuclei are shown in blue. **(C, D)** Quantification of HCMV infection in DOs or TOs infected with AD169r (C) or TB40E (D). Between 75-150 organoids were imaged and HCMV infection scored as at least one positive cell per organoid. Shown are the proportion of organoids that were positive for HCMV. **(E)** Quantification of HCMV (AD169r strain) infection in cells staining positive for HLA-G in TOs. Shown is the percentage of total cells that were positive for HCMV and positive or negative for HLA-G (HLA-G^+ or HLA-G^-, respectively). **(F)** Representative confocal micrographs of TOs infected with EGFP-tagged AD169r and co-immunostained for HLA-G (in red). DAPI-stained nuclei are shown in blue. In A-B, scale bar, 50 µm.

Figure 7

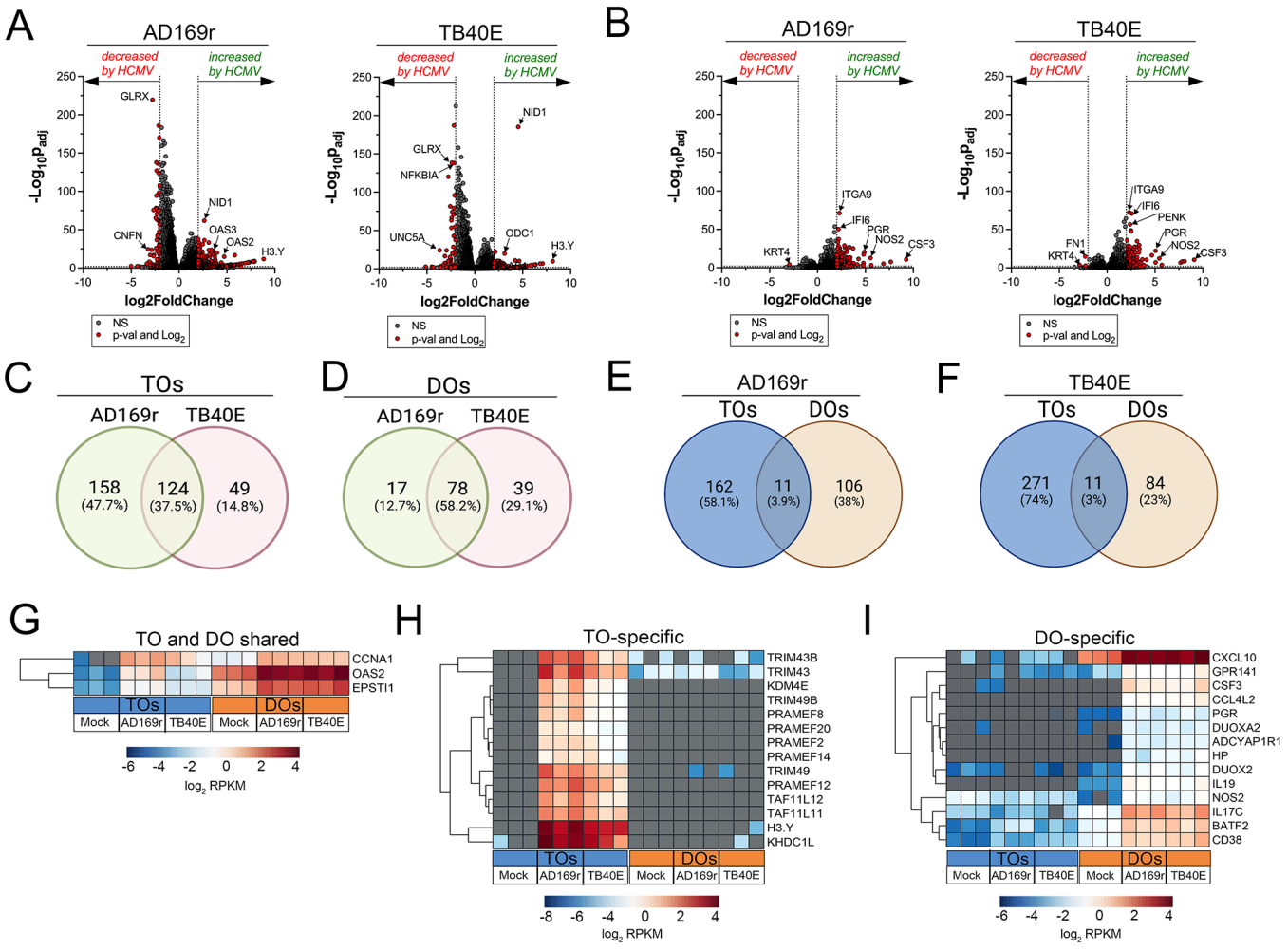

Figure 7. Transcriptional profiling of HCMV infected TOs and DOs. (A, B) Volcano plots demonstrating differentially expressed transcripts in trophoblast organoids (TOs, A) or decidua organoids (DOs, B) infected with HCMV strains AD169r or TB40E (as denoted at top) by DeSeq2 analysis. Grey circles represent genes whose expression was not significantly changed and red denotes transcripts significantly changed by HCMV infections. Significance was set at $p<0.01$ and log2 fold-change of +/- 2. **(C, D)** Venn diagrams of differentially expressed transcripts in TOs (C) or DOs (D) infected with HCMV AD169r (green circle) or TB40E (red circle) strains. **(E, F)** Venn diagrams of the extent of overlap in differentially expressed transcripts in TOs (blue circle) or DOs (orange circles) infected with HCMV AD169r (E) or TB40E (F) strains. **(G)** Heatmap (based on log2 RPKM values) of transcripts induced by HCMV infection of both TOs (blue box, bottom) or DOs (orange box, bottom). **(H, I)** Heatmap (based on log2 RPKM values) of transcripts induced by HCMV infection specifically in TOs (H) or DOs (I). In G-I, key at bottom and red indicates high levels of expression, blue indicates low levels of expression, and grey indicates no reads detected. Hierarchical clustering is on the left.

1042 **Figure 8**

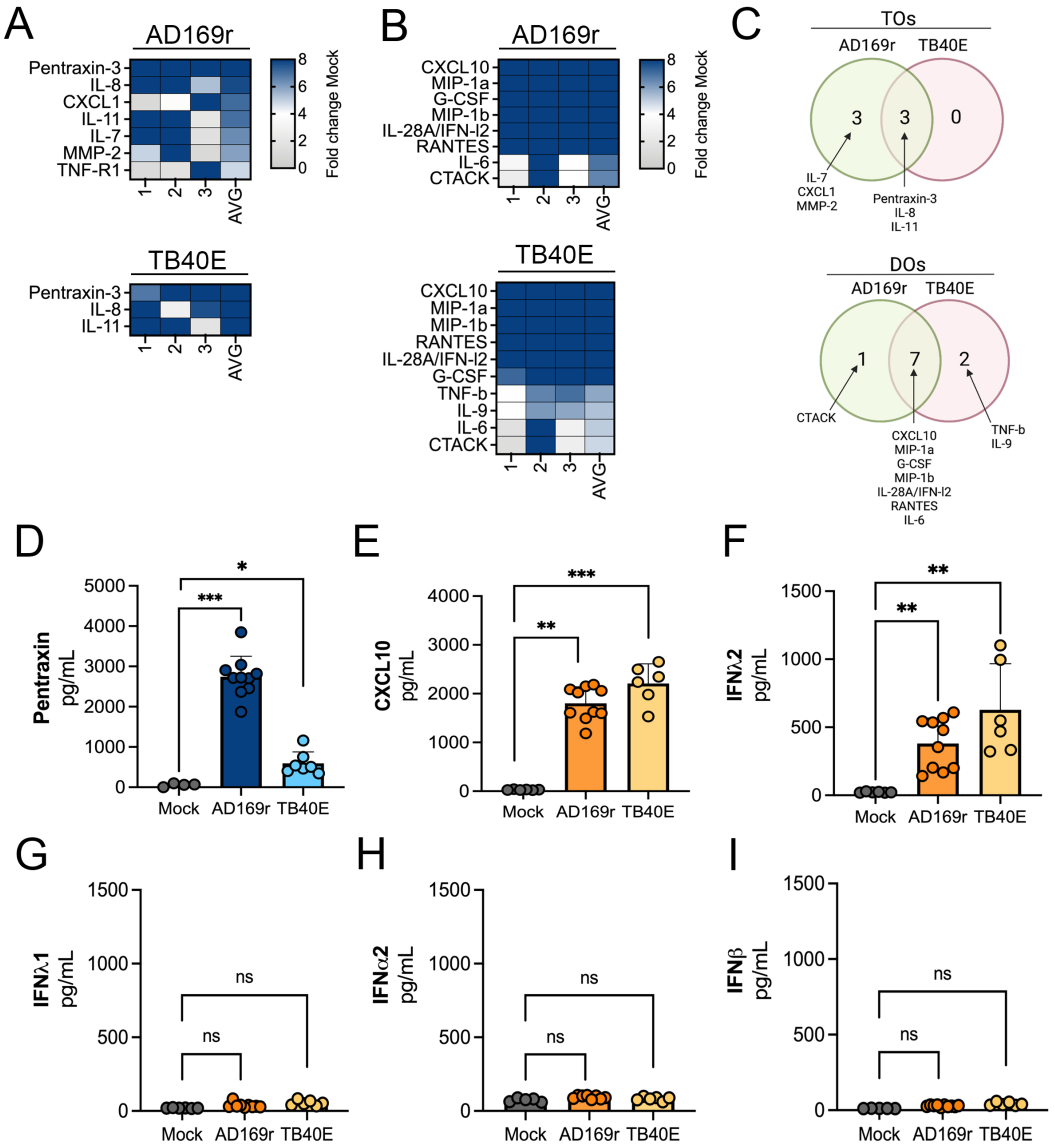

1043
1044

1045 **Figure 8. Differential innate immune responses to HCMV infection of TOs and DOs. (A, B)**
1046 Heatmaps demonstrating the induction of factors at left (shown as fold change from mock-treated
1047 controls) from TOs (A) and DOs (B) infected with HCMV (AD169r, top or TB40E, bottom strains).
1048 Shown are factors induced >5-fold (full heatmap is shown in Supplemental Figure 5). AVG denotes
1049 the average change in concentration of factors over conditioned medium (CM) isolated from three
1050 individual preparations. Dark blue denotes significantly induced factors compared with untreated
1051 controls. Gray or white denotes little to no change (scale at top right). **(C)** Venn diagrams comparing
1052 the factors induced by infection of TOs (top) or DOs (bottom) with AD169r (green) or TB40E (red).
1053 **(D)** Levels of pentraxin in TOs infected with AD169r (middle, dark blue) or TB40E (right, light blue)
1054 compared to mock-infected controls (left, grey). **(E-I)** Levels of CXCL10 (E), IFN-λ2 (F), IFN-λ1 (G),
1055 IFN-α2 (H), or IFN-β (I) in CM isolated from DOs infected with HCMV AD169r (middle, dark orange)
1056 or TB40E (right, light orange) or in in mock-treated controls (left, grey). In D-I, each symbol

represents individual CM preparations and significance was determined using a Mann-Whitney U test. *** $P < 0.001$, ** $P < 0.01$, * $P < 0.05$, ns, not significant.

1104 **Supplemental Figure 1**

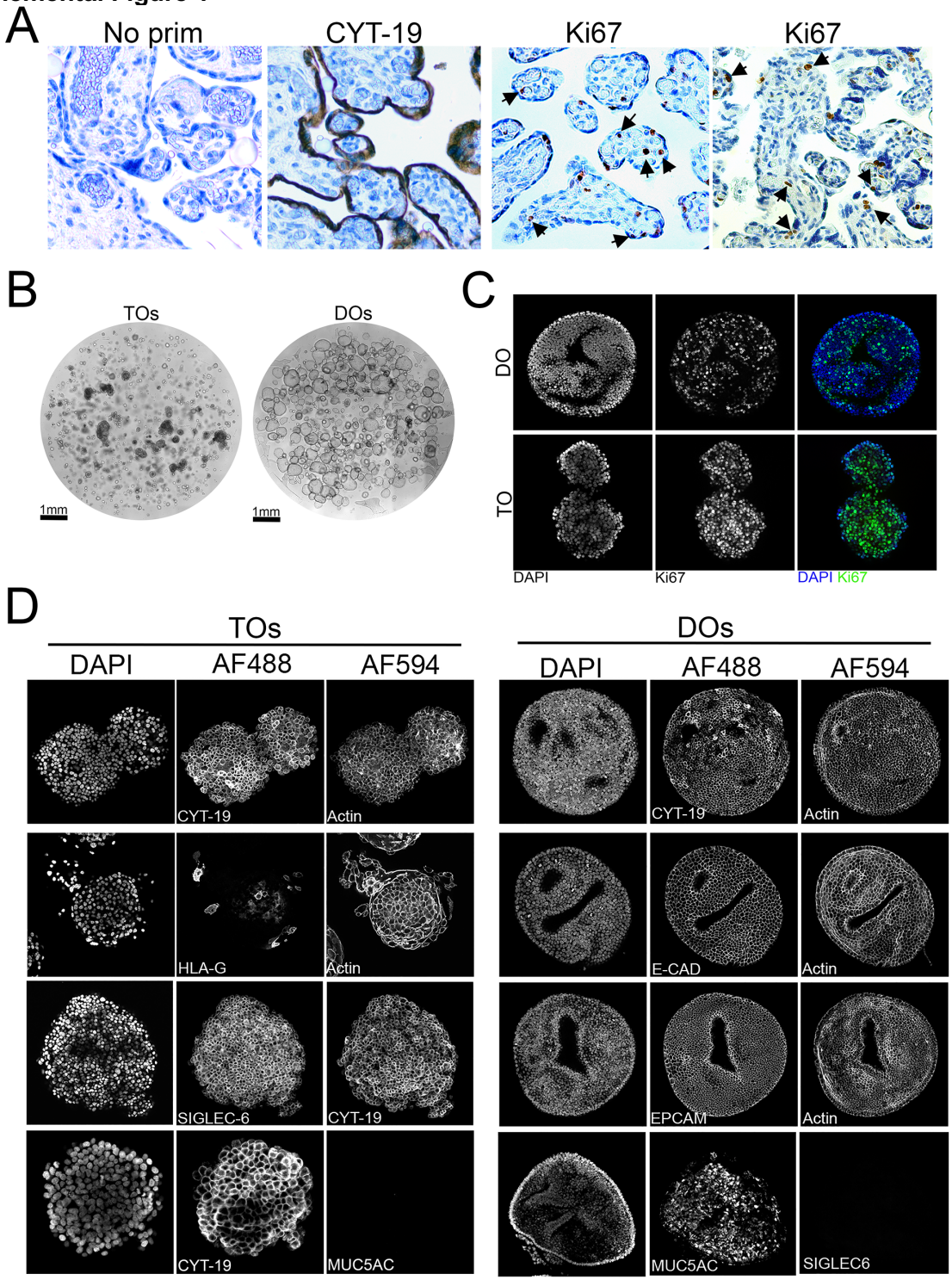

1105
1106 **Supplemental Figure 1. Characterization of trophoblast and decidua organoids. (A)**
1107 Immunohistochemistry in human full-term placental villi tissue used to generate trophoblast
1108 organoids. Shown are no primary controls (left) and representative images of tissue immunostained
1109 for cytokeratin-19 (CYT-19) or Ki-67 as a marker of cell proliferation. Black arrows denote nuclei
1110 positive for Ki-67. **(B)** Brightfield images of Matrigel containing TOs (left) or DOs (right). Tiled images

were captured using a motorized xy-stage at 10x magnification. Scale shown at bottom left. **(C)** Immunostaining for Ki67 (green) in DOs (top) or TOs (bottom). DAPI-stained nuclei are shown in blue. **(D)** Black and white images of single channel confocal micrographs used to generate the merged images shown in Figure 1C and D.

Supplemental Figure 2

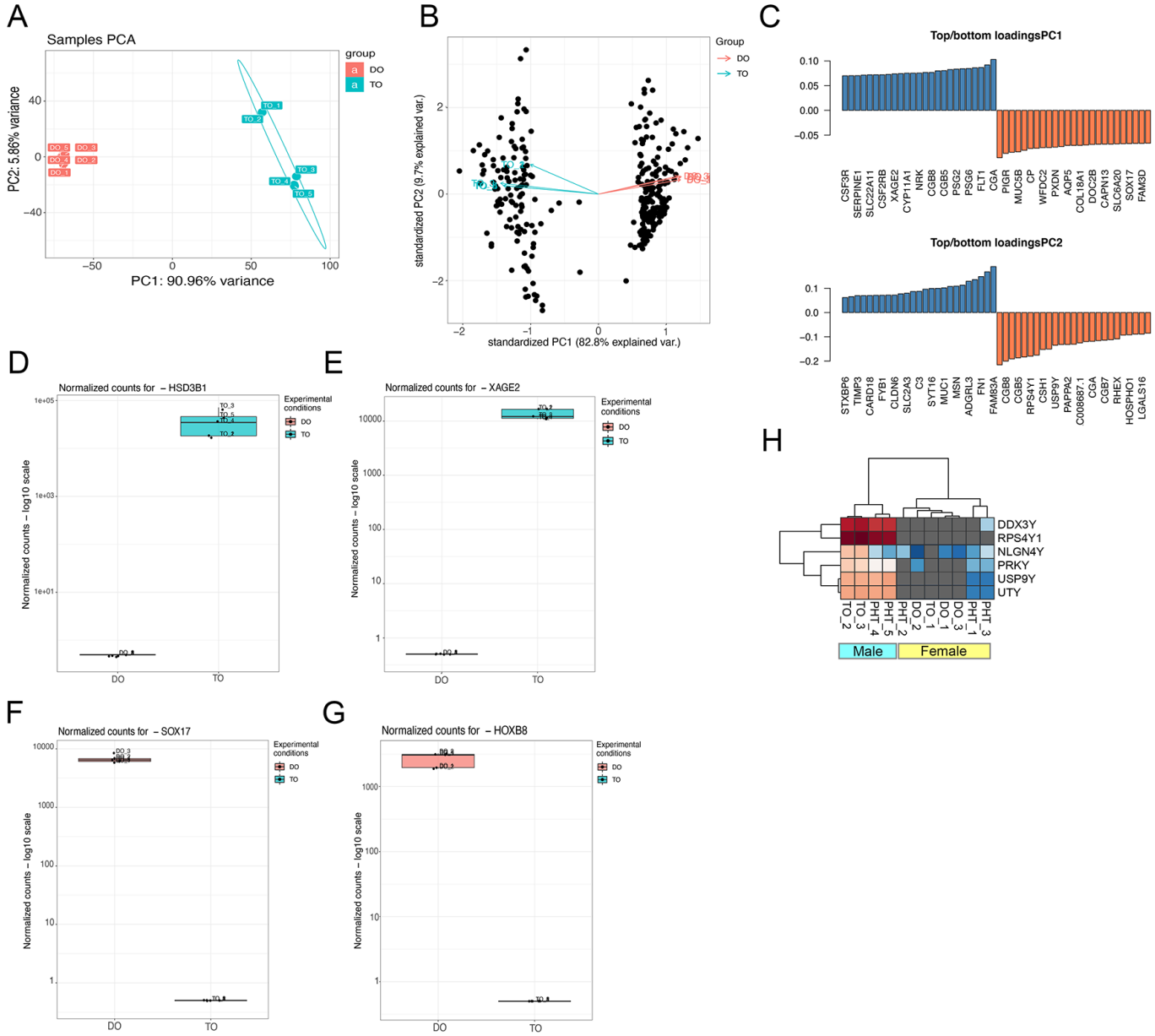

Supplemental Figure 2. RNASeq of TOs and DOs. (A, B) Principal component analysis based on transcriptional profiles from DOs (orange) or TOs (blue**). (C)** Transcripts on the first and second principal components (PC1, PC2) with the greatest variance. Blue indicates enrichment in TOs and orange indicates enrichment in DOs. **(D-G)** Gene-specific enrichment of select transcripts in TOs (blue) and DOs (orange). Shown are HSD3B1 (D), XAGE2 (E), SOX17 (F), and HOXB8 (G). Five individual samples are shown as unique datapoints. **(H)** Heatmap (based on log2 RPKM values) of representative Y-linked transcripts in TOs, DOs, or primary human trophoblasts (PHT). Red indicates high levels of expression, blue indicates low levels of expression, and grey indicates no reads detected. Hierarchical clustering is shown at top.

Supplemental Figure 3

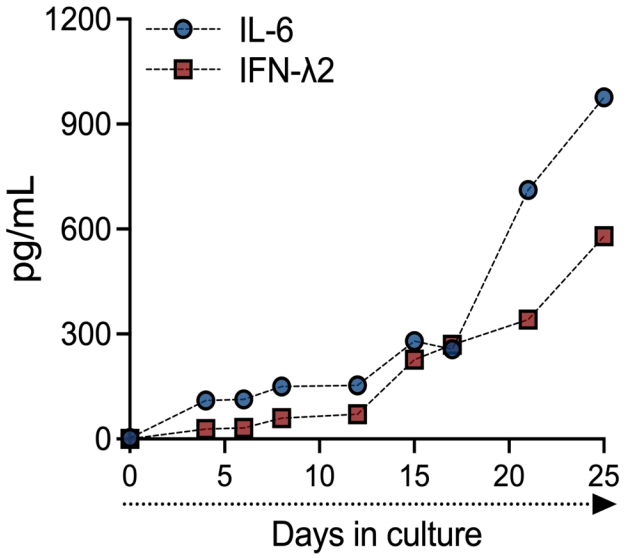

Supplemental Figure 3. IL-6 and IFN-λ2 release in TOs over time. Concentrations of IL-6 (blue) and IFN-λ2 (red) in CM generated from a single TO line throughout the first 25 days of culture.

Supplemental Figure 4

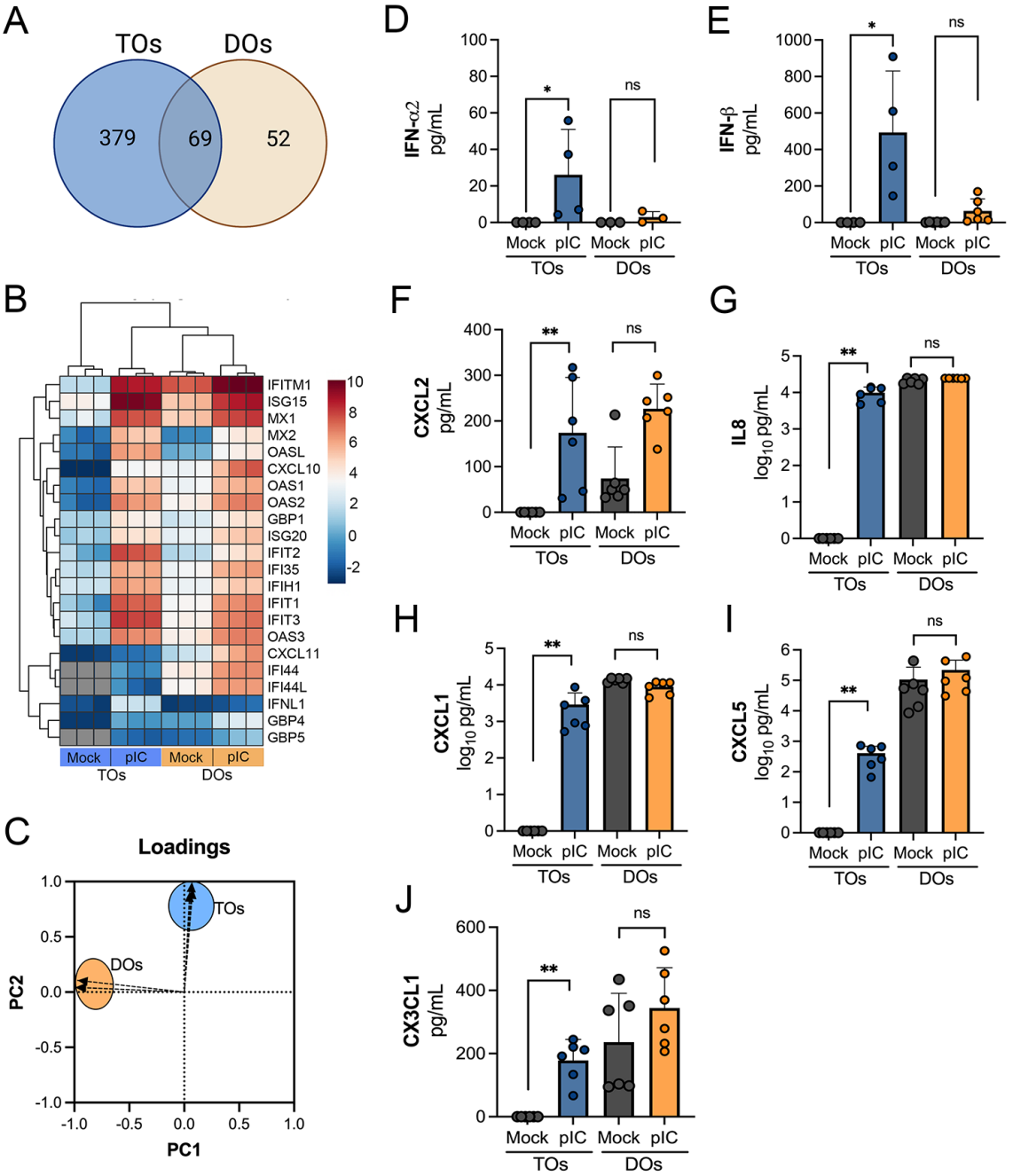

Supplemental Figure 4. Factors induced by poly I:C treatment of TOs and DOs. **(A)** Venn diagram denoting unique and shared differentially expressed transcripts in TOs (blue circle) or DOs (orange circle) treated with poly I:C. **(B)** Heatmap (based on $\log_2$ RPKM values) of transcripts induced by poly I:C treatment of both TOs (blue box, bottom) or DOs (orange box, bottom). Key at

right. Red indicates high levels of expression, blue indicates low levels of expression, and grey indicates no reads detected. Hierarchical clustering is on the left. **(C)** Loadings of principal component analysis of Luminex-based multianalyte profiling of poly I:C treated TOs (blue circle) and DOs (orange circle). **(D-J).** Levels of IFN-α2 (D), IFNβ (E), CXCL2 (F), IL-8 (G), CXCL1 (H), CXCL5 (I), and CX3CL1 (J) in CM isolated from poly I:C-treated TOs (blue) or DOs (orange) or in mock-treated controls (grey). Each symbol represents individual CM preparations. Significance was determined using a Mann-Whitney U test. ** $P < 0.01$, * $P < 0.05$; ns, not significant.

Supplemental Figure 5

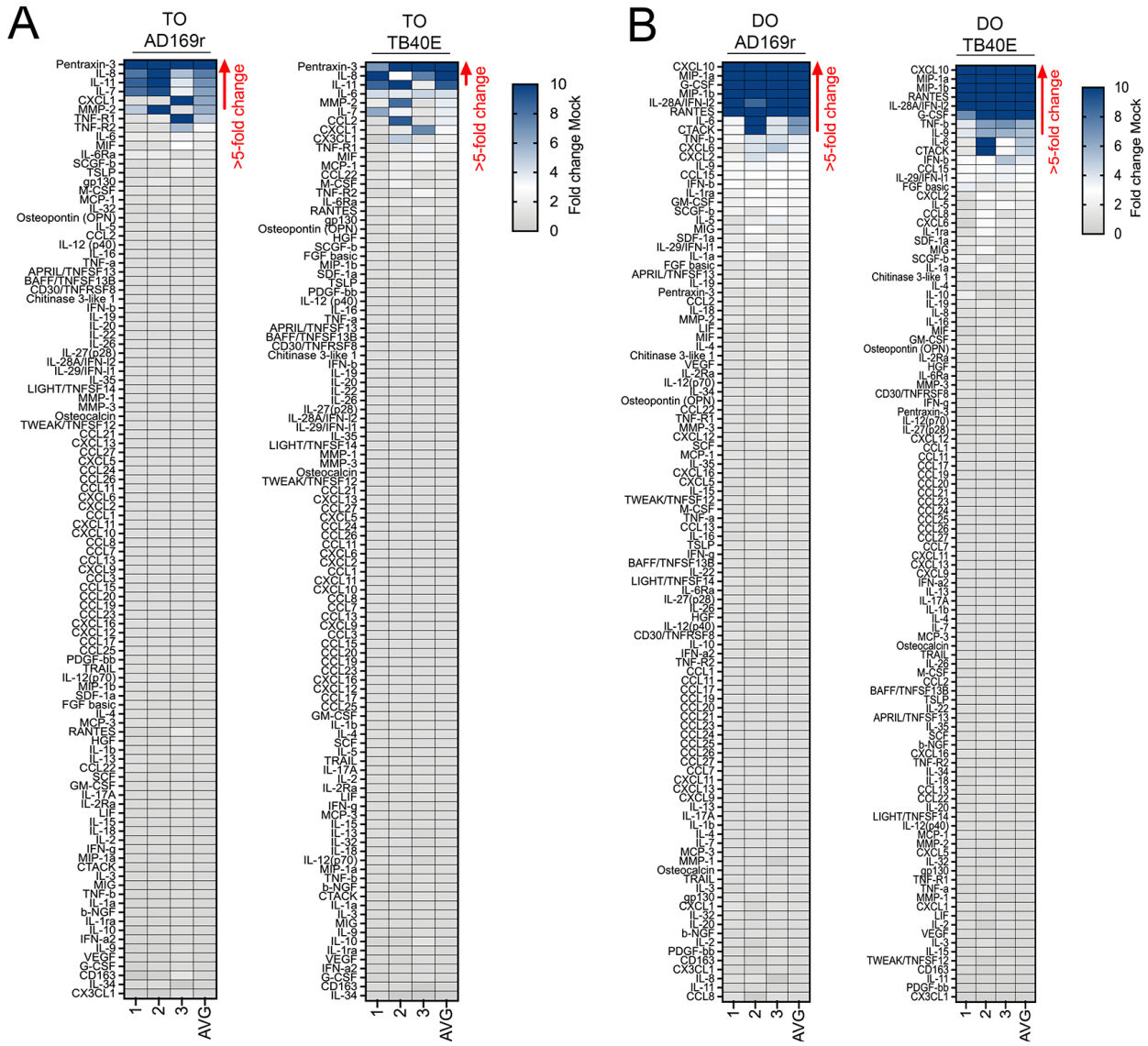

Supplemental Figure 5. Differential innate immune responses in TOs and DOs infected with HCMV. (A, B) Heatmaps demonstrating the induction of factors at left (shown as fold change from mock-treated controls) from TOs (A) and DOs (B) infected with AD169r (left) or TB40E (right) strains of HCMV for ~48hrs as assessed by Luminex-based multianalyte profiling. AVG denotes the average change in concentration of factors over conditioned medium (CM) isolated from three individual preparations. Dark blue denotes significantly induced factors compared with untreated controls. Gray or white denotes little to no change (scale at top right). The red arrow demonstrates factors with induction greater than five-fold change observed in the average of separate experiments.